Journal of Sedimentary Research

Journal of Sedimentary Research, 2020, v. 90, 533–560
Research Article
DOI: http://dx.doi.org/10.2110/jsr.2020.25

FACIES HETEROGENEITY AND SOURCE POTENTIAL OF CARBONATE-MUDSTONE-DOMINATED DISTAL RAMP DEPOSITS, AGRIO FORMATION, NEUQUÉN BASIN, ARGENTINA

SHAWN A. MOORE,*[1] LAUREN P. BIRGENHEIER,[1] MATTHIAS D. GREB,[†2] DANIEL MINISINI,[3,4] MAÍSA TUNIK,[5] AND JULIETA OMARINI[5]

[1]*Department of Geology and Geophysics, University of Utah, FASB, 115 S 1460 E, Room 383, Salt Lake City, Utah 84112-0102, U.S.A.*
[2]*Energy and Geoscience Institute, University of Utah, 423 Wakara Way, Suite 300, Salt Lake City, Utah 84108, U.S.A.*
[3]*Shell Exploration and Production, 150 N Dairy Ashford Road, Houston, Texas 77079, U.S.A.*
[4]*Shell Houston Technology Center, 3333 Highway 6 South, Houston, Texas 77082, U.S.A.*
[5]*Instituto de Investigación en Paleobiología y Geología (CONICET-UNRN), General Roca, Río Negro, Argentina*
e-mail: shawn.a.moore@utah.edu

ABSTRACT: **The carbonate-mudstone-dominated Lower Cretaceous Agrio Formation is the youngest marine source rock of the hydrocarbon-prolific Neuquén Basin in Argentina, yet its facies variability and unconventional hydrocarbon potential remains relatively understudied. Detailed studies of mudstone facies variability in thick, carbonate mudstone successions deposited largely below storm wave base (i.e., chalk–marl, black shale, limestone), like the Agrio Formation, are rare and instead commonly focus on biostratigraphy or organic geochemistry alone. A continuous northern section of the Agrio Formation and a southern composite section of the lower Pilmatué and middle Avilé members, totaling ~ 1,200 m of outcrop, were measured. From these measured sections, programmed pyrolysis (n = 339 samples), X-ray diffraction (XRD; n = 69), and thin sections (n = 69) were used to develop a high-resolution integrated macrofacies and microfacies scheme. The four most volumetrically abundant facies include detrital-quartz-silt-bearing fine mudstone (facies 1), radiolarian-bearing calcareous fine mudstone (facies 2), detrital-quartz-silt- and shell-bearing calcareous fine mudstone (facies 3), and calcareous wackestone (facies 4). All four facies are volumetrically dominated by carbonate mud matrix (i.e., micrite) that represents either 1) original pelagic coccolithophore deposition modified by diagenesis, 2) transported carbonate mud (i.e., bottom currents like contour currents or sediment gravity flows), or 3) a combination of both. Outcrop observations, XRD mineralogic trends, and petrographic variations in grain composition between detrital quartz silt, radiolarian and microfossil to macrofossil content (mainly benthic foraminifera and bivalves) distinguish the four mudstone facies. The facies scheme indicates distinctly more heterogeneous and current-influenced sedimentation in the downdip sub-storm wave base than previously described in the Agrio and in carbonate-dominated basinal settings in general. A depositional model is proposed for further testing that may prove valuable towards re-evaluating basinal carbonate mudstone successions worldwide. Utilizing TOC, S2, and HI value cutoffs, this study defines five discrete stratigraphic packages in the Agrio Formation that have the highest source potential, collectively totaling ~ 140 m thick. The novel integration of macrofacies and microfacies analysis, stratigraphy, and a geochemical analysis allow both depositional insights and the assessment of a potential source rock. The study adds to a growing body of literature on 1) carbonate ramp (or slope) to basinal processes and 2) facies models for organic-rich, carbonate-dominated mudstone successions that are unconventional hydrocarbon systems.**

INTRODUCTION

Mesozoic, organic-rich carbonate mudstone successions deposited in carbonate ramp (or slope) to basinal settings (i.e., chalk–marl, black shale, limestone) are common worldwide and are increasingly viewed as valuable unconventional hydrocarbon resources. Examples include the Eagle Ford and Niobrara of the Cretaceous Western Interior Seaway (U.S.A.), the Haynesville Shale of the east Texas and north Louisiana salt basins (U.S.A), the Vaca Muerta Formation of the Neuquén Basin (Argentina), the Hanifa and Tuwaiq Mountain formations of the Arabian Basin (Saudi Arabia), and North Sea Chalk plays (Back et al. 2011; Hammes et al. 2011; Sonnenberg 2011; Kietzmann et al. 2014, 2016; Al Ibrahim et al. 2017; Minisini et al. 2018). These systems, though mostly deposited in relatively shallow seaways, were deposited largely below storm wave base and are considered pelagic rather than neritic carbonate systems. Previous studies of organic-rich, carbonate mudstone successions (chalk-marls or shale–limestones) have largely focused on biostratigraphy or organic geochemistry, rather than facies variability and depositional mechanisms, resulting in relatively simplistic facies models of these environments that include a pelagic biogenic carbonate mud factory with varying degrees of detrital-

* Present Address: Hess Corporation, 1501 McKinney Street, Houston, Texas 77010, U.S.A.
† Present Address: Devon Energy Corporation, 333 West Sheridan Avenue, Oklahoma City, Oklahoma 73102, U.S.A.

Published Online: May 2020
 1527-1404/20/090-533

clay dilution (i.e., chalks and marls) (e.g., Aguirre-Urreta et al. 2005; Tyson et al. 2005; Back et al. 2011; Sonnenberg 2011). With the exception of Al Ibrahim et al. (2017), integrating detailed sedimentology and geochemistry is relatively rare in the broader literature. In contrast to previous models that depict mud-dominated systems as recording quiet depositional conditions with mud settling slowly out of suspension, many of these systems are now considered to be current-influenced with a broad range of sedimentation rates and more variable energy conditions (Bhattacharya and MacEachern 2009; Plint et al. 2009; Schieber and Yawar 2009; Macquaker et al. 2010a; Zeller et al. 2015; Schieber 2016).

A basic, early understanding of unconventional plays purported that, in contrast to conventional plays, the source, reservoir, and seal rock occupy a common stratigraphic unit (Schmoker 2002; Zou et al. 2013; Zhao et al. 2019). However, a closer inspection at the bed or even pore scale indicates that intraformational migration between source intervals and carrier (reservoir) beds is an important factor to consider in many unconventional plays, particularly in thick mudstone successions (Abrams and Thomas in press). For instance, many leading carbonate-rich unconventional plays, including the Eagle Ford, Niobrara, and, at a larger scale, the Bakken and Three Forks, display organic-rich intervals with source or hydrocarbon-generation potential as well as reservoir intervals that display increased porosity and permeability and/or brittle behavior conducive to hydraulic fracturing and production (Johnston et al. 2010; Sonnenberg 2011; Taylor and Sonnenberg 2014; Breyer 2016; Hogancamp and Pocknall 2018). Therefore, hydrocarbon generation (source quality) should be evaluated separately from hydrocarbon storage and production (reservoir) in mudstone successions.

The Early Cretaceous Agrio Formation of the Neuquén Basin, Argentina, is an ideal candidate on which to conduct a detailed, integrated sedimentologic, stratigraphic, and organic geochemical study due to the accessibility of thick, well-exposed carbonate mudstone deposits (historically described as interbedded organic-rich shales, marls, and limestones) in the outcrop area in northernmost Neuquén province (qualities rare for exposures of mudstone-dominated successions).

Despite the importance of the Agrio Formation as being one of three marine source rocks in the Neuquén Basin, the unconventional hydrocarbon potential of this unit remains relatively understudied. Though extensive biostratigraphic, sedimentary, and stratigraphic studies have been performed on the formation, there has been little integration of these analyses with multiproxy geochemical and geomechanical assessments.

Previous studies indicate that, throughout the basin, the upper and lower members of the Agrio Formation record siliciclastic shoreface to basinal carbonate deposits in an open marine ramp (Legarreta and Uliana 1991, 1999; Spalletti et al. 2001a, 2001b; Lazo et al. 2005; Lazo 2006, 2007a, 2007b). Older, more general stratigraphic and sedimentological studies and several more recent sedimentary-facies studies (e.g., Spalletti et al. 2011; Comerio et al. 2018; Schwarz et al. 2018) provide a comprehensive description of the current facies models for the Agrio Formation throughout the Neuquén Basin, based largely on previous work done 40 to 100 km south of this study's southernmost locality (Fig. 1A). It is well established that the Agrio Formation represents a marine ramp environment with siliciclastic deposits dominating more paleoshore proximal regions in the southern Neuquén region and carbonate deposits dominating more distal basinal regions in the northern Mendoza region (Fig. 2; Legarreta and Uliana 1991, 1999; Sagasti 2002, 2005; Lazo et al. 2005). In this study, we focus on detailed descriptions of the facies from the more distal carbonate-rich northern part of the Neuquén province. This distal, northern part of the basin is also where the highest potential organic richness is predicted (Legarreta and Uliana 1991; Uliana and Legarreta 1993; Cruz et al. 1996; Kozlowski et al. 1998; Uliana et al. 1999). The most distal facies in the Agrio Formation are underrepresented in many facies studies and are usually described as interbedded shales, marls, and limestones (Spalletti et al. 2001a, 2001b; Lazo et al. 2005; Spalletti et al. 2011). Due to high variability in the descriptions used for fine-grained sedimentary rocks between various studies, these terms can be problematic and do not best capture the heterogeneity of these deposits.

The goals of this study are: 1) categorize facies variability in the distal part of the Agrio system (i.e., chalk–marl, black shale, limestone) by integrating macrofacies, microfacies, and geochemical analyses, 2) utilize this understanding of facies heterogeneity to propose a depositional model for further testing, and 3) establish the source potential of these distal deposits in the context of the facies and stratigraphic framework. Establishing the relationship between facies, depositional environment, and source quality better informs play prospectivity of the unconventional Agrio Formation. More broadly, this study provides an integrated method of defining facies, depositional mechanisms, and the hydrocarbon potential of source rock that is analogous to carbonate-dominated mudstone successions of interest worldwide, particularly those of Mesozoic age. This study moves away from a long-standing depositional interpretation paradigm of a simplistic, hemipelagic depositional model resulting in chalk–marl cyclicity and towards a more complex paleogeographic reconstruction of dynamic currents that operated below storm wave base in a carbonate-dominated environment.

GEOLOGIC BACKGROUND AND STUDY AREA

The retroarc Neuquén Basin (35–39° S lat. to 69–70° W long.) was initiated as a rift basin in the Late Triassic and is the thickest rift fill of a linked system of northwest–southeast-trending extensional basins in west-central Argentina (Urien et al. 1995; Aguirre-Urreta et al. 1999; Ramos and Folguera 2005) (Fig. 1A). From the Late Triassic to the Early Jurassic the Neuquén Basin was characterized by intraplate extension and a resulting system of long, narrow half grabens. From the Early Jurassic through the Early Cretaceous, the basin was characterized by widespread protracted thermal, backarc subsidence related to oceanic-plate subduction below the western margin of Gondwana and the emplacement of the Andean magmatic arc. The Andean magmatic arc was nearly fully developed by the Late Jurassic (Howell et al. 2005). Previous studies hold that sedimentation during the Late Jurassic and Early Cretaceous was affected by widespread transgressive–regressive cycles of varying magnitude, which were the result of a combination of eustatic oscillations and tectonic factors such as local uplift and changes in subsidence rates (Legarreta and Uliana 1991; Vergani et al. 1995; Burgess et al. 2000). During this time, more than 4000 m of marine and continental, carbonate, siliciclastic, and evaporitic sediments were deposited. The 120,000 km^2 marine embayment in which the Agrio Formation was deposited formed by the Early Cretaceous. This embayment was bordered by the Andean magmatic arc along its western margin where it connected to the proto–Pacific Ocean and is described as triangular in shape (in plan view) with a low-gradient depositional surface and a shallow-water depositional environment (Fig. 2; Legarreta and Gulisano 1989; Legarreta and Uliana 1991, 1999; Howell et al. 2005; Lazo et al. 2008). From the Late Cretaceous to the Cenozoic, acceleration of plate convergence along the western margin of South America resulted in compression and the evolution of a foreland basin in the Neuquén Basin, closing the embayment. Throughout the basin's formation, its expansion was limited to the northeast by the Sierra Pintada System and to the south by the North Patagonia Massif (Fig. 1A; Vergani et al. 1995; Howell et al. 2005; Ramos and Folguera 2005). The uplift that formed the present-day structure of the outcrops examined in this study occurred in two main phases—a phase of continuous contractional deformation from the Late Albian to the Late Lutetian (~ 100–40 Ma) and a second continuous contractional deformation phase from the Miocene onward (~ 25 Ma onward) (Tunik et al. 2010; Rainoldi et al. 2014; Sánchez et al. 2018).

The Agrio Formation is part of a large Mesozoic sedimentary cycle known as the Middle Supersequences and makes up the majority of the

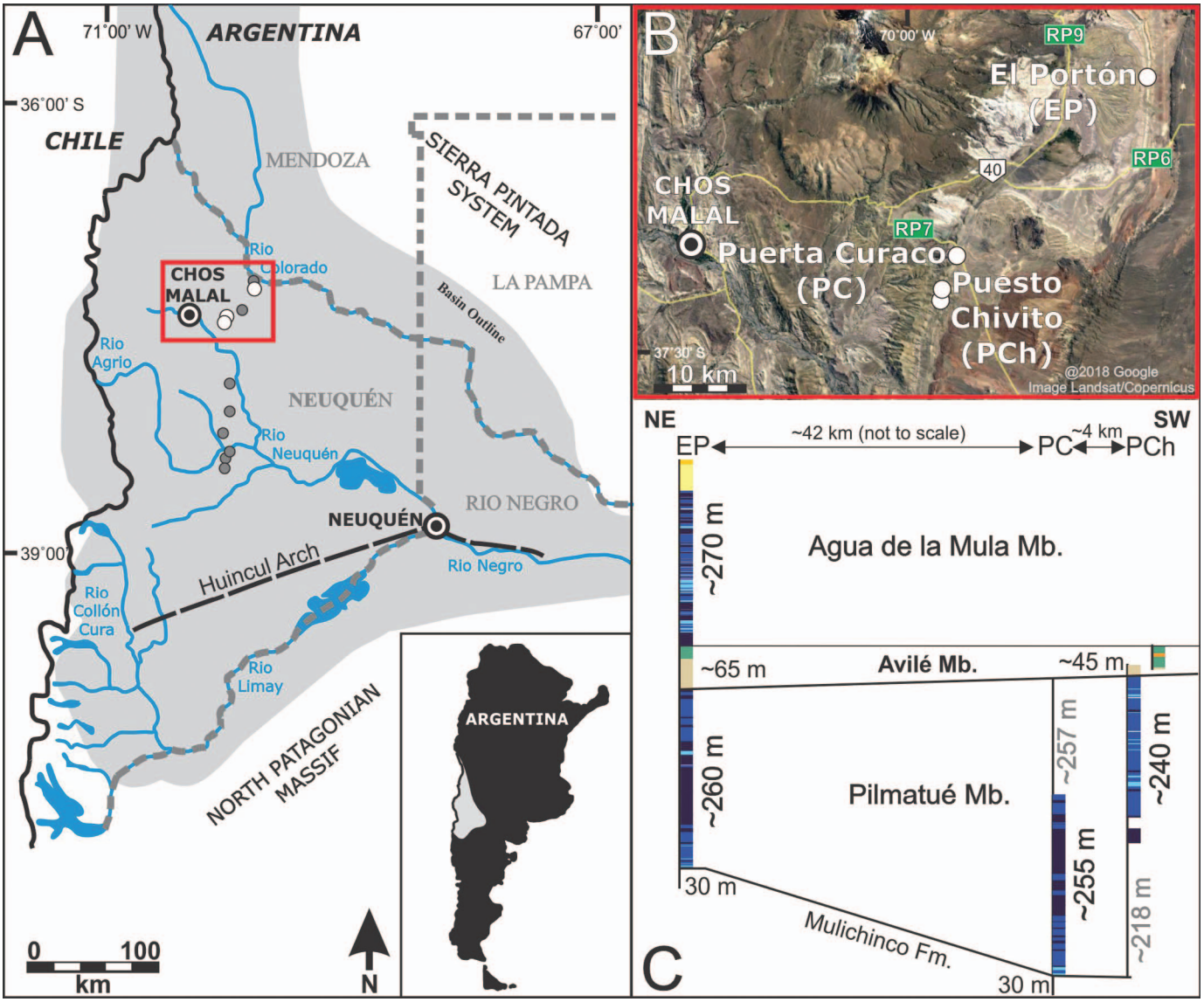

FIG. 1.—**A)** Location map of the Neuquén Basin (gray polygon) with the study area in a red box. Province borders are dashed gray lines. Adapted from Vergani et al. (1995) and Kietzmann et al. (2016). The localities of this study are marked by white dots and previous sedimentological studies reviewed by Spalletti et al. (2011) are marked by gray dots. **B)** Google Earth image of the study area with major towns and roads marked. The localities of this study are marked with white dots. **C)** Stratigraphic correlation of the outcrops measured in this study, showing the members present and stratigraphic height measured at each locality. Stratigraphic heights shown in gray were calculated from thickness and dip angle where section was missing. Outcrop sections are represented by their interpreted depositional environments (see Fig. 4 for key). The contact between the Avilé and Agua de la Mula members is the datum horizon.

Middle and Upper Mendoza Mesosequences (Fig. 3). These sequences were established based on basin-wide assessments of transgressive–regressive cycles (Gulisano et al. 1984; Legarreta and Gulisano 1989). The Lower Cretaceous (Early Valanginian to Latest Hauterivian or Earliest Barremian) Agrio Formation was deposited over a maximum of ~ 10 My from 136 to 126 My (Aguirre-Urreta et al. 1999, 2017; Sagasti and Ballent 2002) and is the youngest of the three main source rocks of the Neuquén Basin. The older two are the Early–Middle Jurassic Los Molles Formation and the Late Jurassic to Earliest Cretaceous Vaca Muerta Formation, the latter of which is the most prolific hydrocarbon source rock in the basin (Villar et al. 1998; Legarreta et al. 2005; Legarreta and Villar 2012). The Los Molles and Vaca Muerta formations are both being developed as unconventional petroleum systems. The Agrio Formation is an emerging unconventional play. The underlying contact of the marine Agrio Formation with the marginal marine to continental Mulichinco Formation is gradational, but the base of the first thick marine black shale unit is typically taken to mark the diachronous lithostratigraphic contact between the two formations (Aguirre-Urreta and Rawson 1997). The Agrio Formation is unconformably overlain by the siliciclastic and evaporitic beds of the Huitrín Formation, which mark the end of marine-influenced sedimentation in the Neuquén Basin during the Barremian (Urien et al. 1995; Aguirre-Urreta et al. 1999). Three members have been identified in the Agrio Formation. The lower Pilmatué Member and upper Agua de la Mula Member, formally named by Leanza et al. (2001), are generally associated with accumulation during transgressive periods in a slowly subsiding marine ramp environment, and the central sandstone-dominated Avilé Member, named by Weaver (1931), is associated with an abrupt

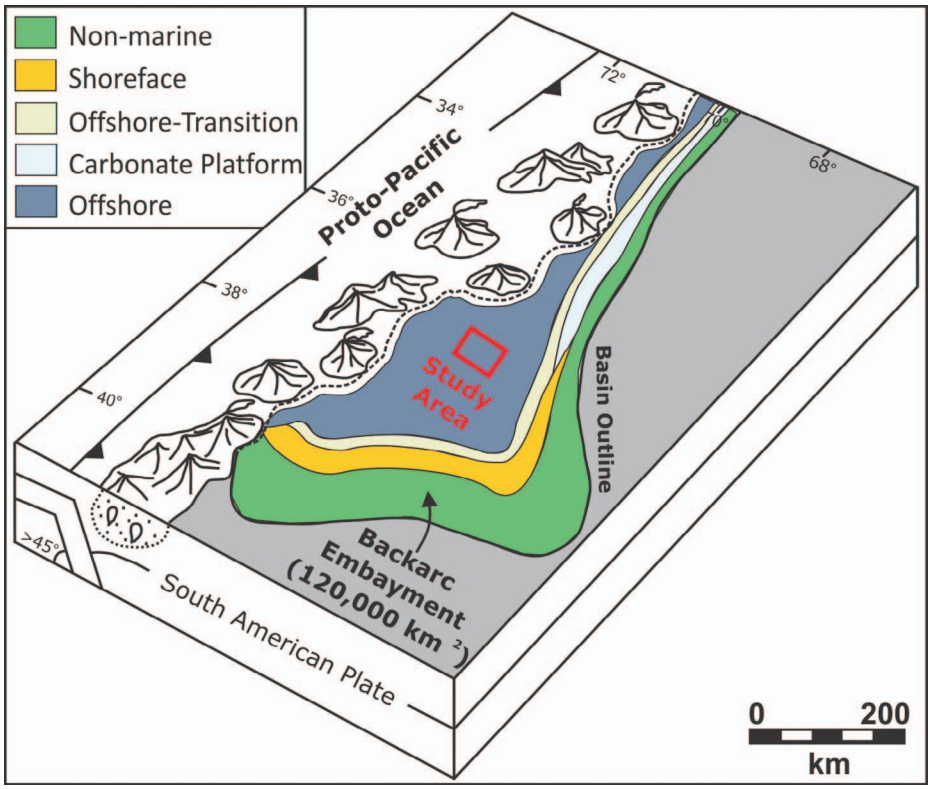

FIG. 2.—Paleogeographic reconstruction of the Neuquén Basin during the Early Cretaceous at the time of Agrio Formation deposition. Adapted from Howell et al. (2005). Overlays of depositional environments are adapted from Spalletti et al. (2011) and Schwarz et al. (2018).

regression that occurred in the mid-Hauterivian (Legarreta and Gulisano 1989; Legarreta and Uliana 1991; Spalletti et al. 2011).

Previous studies indicate that, during deposition of the Agrio Formation, the Neuquén Basin was dominated by coastal to lower-shoreface siliciclastic deposits in the southern to southeastern parts of the basin with a complex carbonate and siliciclastic shoreline forming the eastern margin of the basin (Legarreta and Uliana 1991, 1999; Sagasti 2002, 2005; Lazo et al. 2005; Spalletti et al. 2011) (Fig. 2). Distal marine deposits were restricted to the central and northwestern parts of the basin (Sagasti 2005; Spalletti et al. 2011). These previous paleogeographic reconstructions, though valuable as an overview, have relied on relatively generalized observations from widely spaced localities and have been somewhat model-driven. A closer inspection of the distal environments was needed to describe this region and is provided here. Previous sedimentological studies indicate a homoclinal geometry for this mixed carbonate–siliciclastic ramp, though localized examples of short-term distal steepening have been noted in deposits of the Pilmatué Member (Lazo et al. 2005; Schwarz et al. 2011). The study area of this work is located near the town of Chos Malal (Fig. 1A, B), where the most distal carbonate-rich deposits of the Pilmatué and Agua de la Mula members with the highest predicted organic richness in the Neuquén province are found (Legarreta and Uliana 1991; Uliana and Legarreta 1993; Uliana et al. 1999; Sagasti 2005; Spalletti et al. 2011; Aguirre-Urreta et al. 2017). The Avilé Member is fairly well studied in this area (Rossi 2001; Veiga et al. 2011) and is not the focus of this study.

DATA SET AND METHODS

In order to construct a depositional model for the Agrio Formation and to assess its source potential, this study combines field data from over 1200 m of measured sections from three localities, petrographic analysis of 69 thin sections (~ 20 μm), X-ray diffraction (XRD) analysis on 69 samples, and programmed pyrolysis data from 339 samples.

Four outcrop sections from three localities were measured at the centimeter scale with particular emphasis placed on sedimentary structures, bedding style, trace fossils, and stratigraphic stacking patterns. Moving from north to south, these localities are El Portón (~ 655 m), Puerta Curaco (~ 285 m), and Puesto Chivito (~ 300 m) (Fig. 1B, C). Where outcrop was not continuous and was too weathered to measure, significant member or formation contacts, thickness, and dip angles were utilized to establish stratigraphic thickness. 423 samples were hammered out of the outcrop at an average sampling interval of ~ 2.5 m. Sample spacing varied as outcrop and bed quality allowed (i.e., poorly exposed intervals were skipped altogether). Because outcrop quality did not allow consistent stratigraphic spacing between samples, special attention was paid to collect proportions of different mudstone facies that reflected their overall thickness distribution in outcrop. So the sampling scheme was designed to principally reflect facies proportions and secondarily achieve stratigraphic coverage. Larger sampling intervals were also used through non-mudstone-dominated sections. Every attempt was made to acquire the cleanest sample possible and to collect a representative suite of the facies present. Grain composition, fossil content, bioturbation, and diagenetic features were described in thin section, allowing for a comparison with the outcrop based macrofacies. Grain composition percentages were based on visual estimates. An adaptation of the Lazar et al. (2015) facies naming scheme was utilized in the analyses of both outcrop facies and petrographic facies. Terminology for carbonate mudstone and wackestone is used following Dunham (1962). Modifiers indicate the dominant grains present in each facies, even where grains are rare. The Bioturbation Index (BI) used in macroscale outcrop observations is based on Taylor and Goldring (1993), and the recognition of cryptobioturbation in microscale petrographic observations follows Pemberton et al. 2008 and Wilson and Schieber 2015. The combination of macrofacies and microfacies observations is key to the creation of the unified facies scheme presented herein.

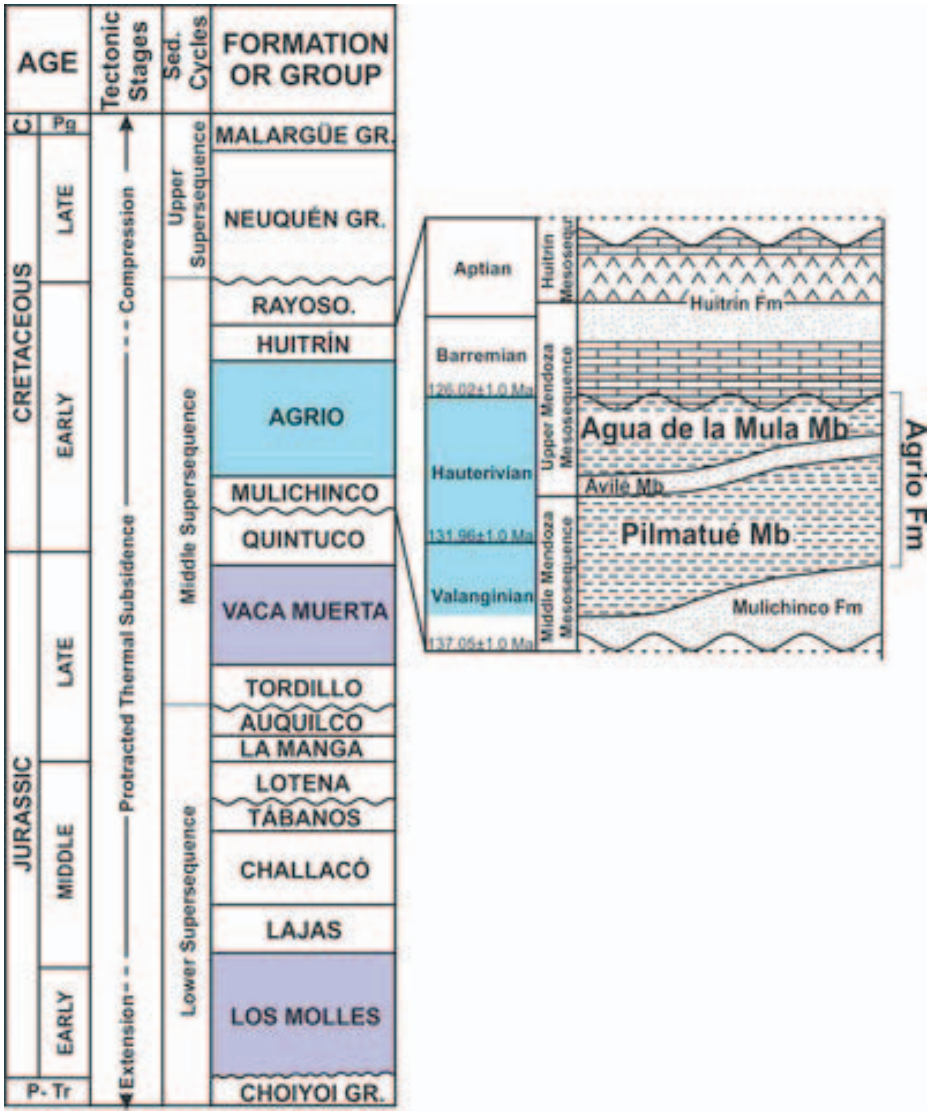

FIG. 3.—Stratigraphic column of the Neuquén Basin, including major tectonic stages and a schematic stratigraphic section of the Early Cretaceous units. Study interval highlighted in blue and older marine source rocks of the Neuquén Basin are highlighted in purple. Adapted from Urien and Zambrano (1994), Aguirre-Urreta and Rawson (1997), Howell et al. (2005), and Veiga et al. (2005). Age dates for the base of the Valanginian, Hauterivian, and Barremian are from Aguirre-Urreta et al. (2017).

Whole-rock and clay XRD analyses were performed using a Bruker D8 ADVANCE X-ray diffractometer at the Energy and Geoscience Institute, University of Utah. When analyzing both the clay-size fraction and the bulk samples, the following calibration parameters were used: Cu Kα radiation at 40 kV and 40 mA, 0.02° 2θ step size, and 0.4 and 0.6 seconds per step, for clay and bulk samples, respectively. Clay samples were examined from beam diffraction angles 2 to 45° 2θ and the bulk samples from 4 to 65° 2θ. At a minimum, three analyses were conducted on each sample—two or more on the clay-sized fraction and one on the bulk sample.

Programmed pyrolysis analysis was performed on the HAWK instrument at Energy and Geoscience Institute, University of Utah. All samples were hand crushed using a mortar and pestle in order to avoid degradation of hydrogen through the frictional heating involved with mechanized crushing methods. An empty crucible, a Wildcat Technologies rock standard, and an internal standard were placed in 25 sample intervals in the run sequence to ensure that acceptable percent error was maintained. A large benefit to conducting programmed pyrolysis using the HAWK instrument is that acid preparation of samples is unnecessary even in samples containing high percentages of carbonate. To ensure that carbonate content did not skew the data produced by the HAWK instrument, a subset of 15 samples were treated with acid and analyzed following industry standard "Bulk-rock/basic" method/cycle procedure on a Rock-Eval 6 device at the StratoChem lab in Cairo, Egypt. Analyses from both methods yielded nearly identical results providing a high confidence in the data derived from the HAWK. This is consistent with findings that the results from the HAWK instrument are comparable to those of other programmed pyrolysis instrumentation (Birdwell et al. 2017).

The main programmed pyrolysis proxies of interest for evaluating source potential and thermal maturity are total organic carbon (TOC), S2 (the remaining generative potential), hydrogen indices (HI), oxygen indices (OI), and Tmax (the temperature of peak hydrocarbon generation during pyrolysis). TOC informs the quantity of organic material, S2 is a proxy for the quality of organic material, and HI and OI are proxies for the type of organic material. Tmax acts as a proxy for thermal maturity.

SEDIMENTARY FACIES AND PROCESSES

Analyses of outcrops, petrographic assessment of thin sections, and XRD were used to establish seven facies in the Pilmatué and Agua de la Mula members (Table 1; Fig. 4). Though four facies specific to the upper 45 m of the Agua de la Mula Member at El Portón and eight facies in the Avilé Member of the Agrio Formation were also established, other studies have focused more directly on describing these siliciclastic-dominated facies with similar results (Legarreta et al. 1981; Veiga and Vergani 1993; Veiga et al. 2002, 2005, 2007, 2011; Tunik et al. 2009; Spalletti et al. 2011). For this reason, and because this study focuses on distinguishing mudstone-dominated facies and environments, only the seven facies specific to the Agua de la Mula and Pilmatué members are addressed herein. Of these seven facies that were identified (Table 1), there are four key facies, all carbonates, that make up the highest volume of the Pilmatué and Agua de la Mula members in the distal ramp part of the basin. Thus, only these four calcareous micritic facies are described in detail below and brief descriptions are provided for less volumetrically significant facies identified in these two members. Supplemental information provides outcrop measured sections (Appendices A, B, C) and detailed descriptions of the mudstone-dominated Pilmatué and Agua de la Mula Member facies not presented in detail (Appendix D).

Facies 1: Detrital-Quartz-Silt-Bearing Fine Mudstone

Detrital-quartz-silt-bearing fine mudstone (fMs), facies 1, is the most volumetrically abundant facies in the Pilmatué and Agua de la Mula members at all localities in this study. Facies 1 constitutes an estimated 50% of the measured sections. In outcrop, facies 1 appears black to gray in color, fizzes in response to hydrochloric acid (i.e., are carbonates), and is recessed with a fissile weathering appearance (i.e., "black shale," Fig. 5A, D). Beds of this facies can be up to 13 m thick, but most commonly they are only a few centimeters thick due to high-frequency interbedding with facies 2, 3, and 7 and, to a lesser degree, facies 4, 5, and 6 (Table 1; Appendix D). No sedimentary structures, bioclastic material, or trace fossils are visible in outcrop other than rare ammonite casts.

In thin section (n = 27), detrital-quartz-silt-bearing fMs is dominated by micritic matrix. The grain fraction accounts for ~ 11% of this facies on average and is dominated by subangular, medium-silt-sized dispersed detrital quartz grains (Figs. 5B, 6). The grain fraction also includes silt-size dispersed bioclastic shell material and rare Radiolaria and Foraminifera. The shell material is largely on the microfossil scale, but some samples include identifiable gastropods, bivalves, echinoid spines, and ostracod macrofossil fragments (Fig. 5C). All bioclastic and biogenic material has been recrystallized, if originally aragonite or calcite, or replaced, if originally siliceous, by drusy and/or blocky spar calcite cement. The sand fraction accounts for less than 3% of the composition of this facies on average but consists largely of partially degraded plagioclase grains (Figs. 5B, 6). Though definitive outlines of individual burrowers are difficult to identify in thin section, visible clotted organic-rich (silt-free) and dispersed detrital-silt-rich domains in thin section suggest that heavy bioturbation characterizes this facies (Fig. 5E). Cryptobioturbation has admixed the sediment and destroyed original sedimentary structures completely (Fig. 5B, E).

XRD analyses on 28 samples of facies 1 indicate that the matrix in the detrital-quartz-silt-bearing fMs is composed of calcite and detrital illite with minor amounts of other detrital clay minerals (Fig. 7A). For all facies, the XRD calcite content represents both carbonate mud and the calcite cement recrystallizing and/or replacing all bioclastic and biogenic material. On average, clay minerals, feldspars, and silica constitute over 55% of facies 1. Only minor amounts of dolomite, pyrite, and other accessory minerals are present.

Programmed pyrolysis results on 155 samples of facies 1 (Table 2) show TOC content ranging from 0.31 to 10.66 wt.% with an average of 1.57 wt.% (Fig. 8A). S2 values range from 0.04 to 70.28 mg HC/g rock with an average of 3.44 mg HC/g rock (Fig. 8B), and HI values ranging from 6 to 709 mg HC/g TOC with an average of 153 mg HC/g TOC (Fig. 8C). Kerogen types inferred from these geochemical proxies range widely from terrigenous- to marine-dominated, with many samples showing a mixed terrigenous and marine signature (Type II/III) or a biodegraded marine (Type II) signature (Fig. 9).

Facies 2: Radiolarian-Bearing Calcareous Fine Mudstone

Radiolarian-bearing calcareous fMs, facies 2, is the second most volumetrically abundant facies in the Pilmatué and Agua de la Mula members at all localities in this study. Facies 2 constitutes an estimated 30% percent of the measured sections. Facies 2 is resistant in outcrop, creating thin to thick (0.03–1.1 m), laterally continuous beds with sharp non-erosional bases. Beds in outcrop fizz in response to hydrochloric acid (i.e., are carbonates) and are commonly referred to as "limestones." These beds are interbedded with facies 1 and are either discrete or grouped in packages, which amalgamate laterally in some cases (Fig. 10A, B). They commonly display a white weathering appearance but are dominantly black beneath on a fresh surface (Fig. 10B). Though largely structureless, rare beds show either continuous planar parallel, discontinuous wavy parallel, or discontinuous wavy nonparallel laminae (Fig. 10C). Bioclastic material is not visible in outcrop, but ammonite casts are common. *Planolites* and *Thalassinoides* trace fossils are uncommonly visible on the upper bedding planes of this facies in outcrop, usually where it is overlain by facies 7 (Table 1; Fig. 10D). BI is most commonly 1, but ranges from 1 to 4 in outcrop.

Radiolarian-bearing fMs is dominated by micritic matrix in thin section (n = 21 total). The grain fraction accounts for ~ 9% of this facies on average and is heavily dominated by very fine-sand-sized Radiolaria that have been completely replaced by blocky spar calcite cement (Fig. 10E, F). The rest of the sand fraction consists of benthic foraminifera, some unidentifiable macrofossil shell material, identifiable macrofossil bivalves, gastropods, echinoderm plates, and rare degraded feldspar grains (Fig. 10–I). The foraminifera assemblage appears polytypic (Fig. 10H, I). The silt fraction consists of approximately equal percentages of medium-silt-size, subangular detrital quartz grains and dispersed microfossil shell material. Rare sponge spicules are also present in some cases. As in facies 1, all bioclastic and biogenic material has been recrystallized or replaced by drusy and/or blocky spar calcite cement. Though detrital silt is not as abundant as in facies 1, it also is completely dispersed in thin sections of facies 2, indicating that the sediment was admixed through heavy cryptobioturbation.

XRD analyses on 24 samples of facies 2 indicates that the matrix of facies 2 is composed mainly of calcite with minor detrital clay minerals, the most common of which is illite (Fig. 7A). On average, clay minerals, feldspars, and silica account for less than 30% of facies 2. Facies 2 has a relatively high percentage of dolomite at ~ 15% as compared with other facies, with very minor amounts of pyrite and other accessory minerals.

Programmed pyrolysis results on 107 samples from facies 2 (Table 2) show TOC content ranging from 0.25 to 3.8 wt.% with an average of 1.20 wt.% (Fig. 8A). S2 values range from 0.06 to 21.29 mg HC/g rock with an average of 3.97 mg HC/g rock (Fig. 8B), and HI values range from 14 to 637 mg HC/g TOC with an average of 262 mg HC/g TOC (Fig. 8C). Kerogen types inferred from these geochemical proxies show a variability and range similar to that of facies 1. However, facies 2 shows a distinct trend of more marine-dominated organic material (Type II) and/or a marine signature with less biodegradation (Fig. 9).

TABLE 1.—*Facies of the Pilmatué and Agua de la Mula members within this study area.*

Facies #	Facies Name	Grain Population	Mineralogical Composition	Outcrop Expression	Bioturbation Index	Process Interpretation	Depositional Environment
1	Detrital- quartz-silt-bearing fine mudstone	Micrite-dominated; grain fraction ~ 11% on average and dominated by detrital quartz grains	Calcareous to argillaceous; micritic matrix composed mainly of calcite and illite; detrital clay minerals, feldspars, and silica constitute > 55% on average	Black to gray; recessed, fissile; beds up to 13 m, but commonly centimeter scale; interbedded with all other facies; no sedimentary structures, bioclastic material, or trace fossils visible in outcrop	5 to 6; crypto-bioturbation in thin section	Shallow marine bottom currents, enhanced sediment gravity flows, minor suspension settling of pelagic material	Present from proximal outer ramp to basinal environments, but characteristic of the distal outer ramp
2	Radiolarian-bearing calcareous fine mudstone	Micrite-dominated; grain fraction ~ 9% on average and dominated by Radiolaria	Calcareous; micritic matrix composed mainly of calcite; detrital clay minerals, feldspars, and silica constitute < 30% on average; ~ 15 % dolomite on average	Black with white weathering face; resistant; beds 0.03–1.1 m, laterally continuous, sharp non-erosional bases; may be discrete or grouped; amalgamating; largely structureless, with rare laminae; bioclastic material not visible in outcrop	5 to 6; crypto-bioturbation in thin section; *Planolites* and *Thalassinoides* trace fossils visible in outcrop	Shallow marine bottom currents, suspension settling of pelagic material, minor enhanced sediment gravity flows	Present from proximal outer ramp to basinal environments, but characteristic of the basinal setting
3	Detrital- quartz-silt- and shell-bearing calcareous fine mudstone	Micrite-dominated; grain fraction ~ 14% on average and dominated by shell fragments and detrital quartz silt	Calcareous; micritic matrix composed mainly of calcite; detrital clay minerals, feldspars, and silica constitute < 25% on average	Gray; semi-resistant; 0.03–0.5 m laterally continuous beds; no sedimentary structures or bioclastic material visible in outcrop.	5 to 6; crypto-bioturbation in thin section	Shallow marine bottom currents, enhanced sediment gravity flows, minor suspension settling of pelagic material	Present from proximal outer ramp to basinal environments
4	Calcareous wackestone	Micrite-dominated; grain fraction ~ 30% on average and dominated by shell fragments and/or foraminifera	Calcareous; micritic matrix composed mainly of calcite; detrital clay minerals, feldspars, and silica constitute ~ 40% on average	Black with white weathering face; resistant; 0.03–1.1 m, laterally continuous beds with sharp non-erosional bases; discrete or grouped; amalgamating; largely structureless, with rare laminae; contains between 5 and 15% bioclastic material	5 to 6; crypto-bioturbation in thin section; *Planolites* and *Thalassinoides* trace fossils visible in outcrop at Puesto Chivito	Shallow marine bottom currents, enhanced sediment gravity flows, minor suspension settling of pelagic material	Characteristic of the proximal outer ramp
5	Calcareous intraclastic packstone	Micrite-dominated; grain fraction ~ 60% on average and dominated by micritic intraclasts	Calcareous; micritic matrix composed mainly of calcite; detrital clay minerals, feldspars, and silica constitute ~ 15% on average	Rare (only seen at El Portón); tabular, laterally continuous beds ~ 0.4 m thick; flaggy bedding; densely packed, round sand-size "grains" visible on the tops of beds; no shell material or trace fossils visible in outcrop	0	Transgressive erosion (?)	N/A
6	Calcareous floatstone	N/A	N/A	Rare (only several beds in the upper section of the Pilmatué member at Puesto Chivito); semi-resistant; laterally discontinuous over more than 10 m; 5–15 cm beds; contains both abundant shell debris (mm-5 cm scale bivalve and gastropod fragments) and large articulated and disarticulated bivalve shells (oyster-dominated mixed assemblage)	0; no thin sections available to identify crypto-bioturbation	Storm related enhanced sediment gravity flows and *in situ* colonization	Characteristic of the more proximal portion of the distal outer ramp
7	Tuff	N/A	N/A	Orangish weathering color; friable; 0.01–0.15 m beds; commonly heavily altered by gypsum; no sedimentary structures visible in outcrop	0; no thin sections available to identify crypto-bioturbation	Distal ash fall and suspension settling	N/A

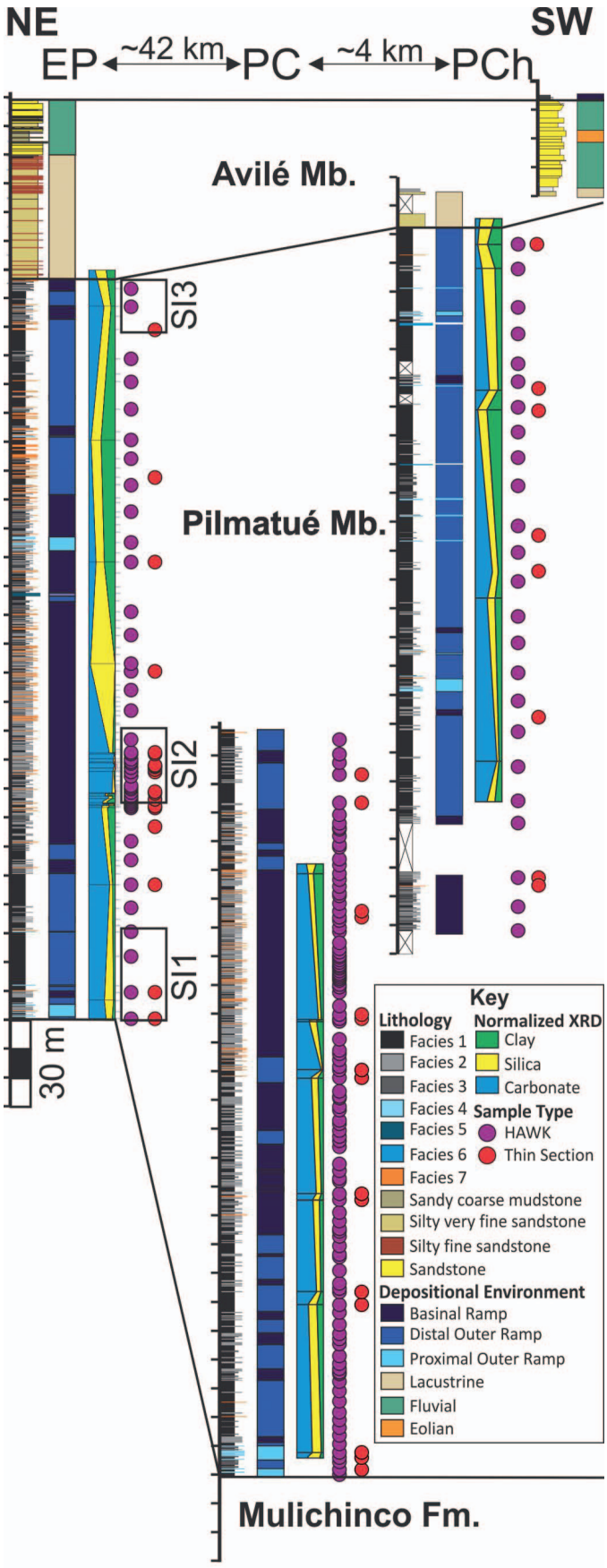

Facies 3: Detrital-Quartz-Silt- and Shell-Bearing Calcareous Fine Mudstone

Detrital-quartz-silt- and shell-bearing calcareous fMs, facies 3, is slightly less volumetrically abundant than facies 2 in the Pilmatué and Agua de la Mula members and is commonly interbedded with facies 1 in outcrop and rarely with facies 2. Facies 3 constitutes an estimated 10% percent of the measured sections. In outcrop, this facies forms semi-resistant, relatively thin (0.03–0.5 m) beds that are generally laterally continuous but are commonly too weathered to distinguish easily from facies 1 (Fig. 5D). These beds fizz in response to hydrochloric acid (i.e., are carbonates). No trace fossils, sedimentary structures, or bioclastic material are visible in outcrop.

Detrital-quartz-silt- and shell-bearing calcareous fMs is dominated by micritic matrix in thin section (n = 8), with the grain fraction accounting for ~ 14% on average. The grain fraction is dominated by a slightly more mixed percentage of bioclastic material and subangular, medium-silt-size, dispersed detrital quartz grains than present in facies 1(Figs. 5E, 6). The bioclastic material is mainly unidentifiable microfossil shell fragments with some gastropod, bivalve, ostracod, and echinoderm plates macrofossil fragments (Fig. 5G, H). Facies 3 also contains elevated percentages of very fine-sand-size Radiolaria and foraminifera compared with facies 1 (Figs. 5H, 6). Foraminifera appear admixed with a mixed assemblage of bioclastic material. As in facies 1 and 2, all carbonate bioclastic and biogenic material has been recrystallized or replaced by drusy and/or blocky spar calcite cement, and all silica Radiolaria have been replaced and filled with calcite. Additionally, syntaxial overgrowths are apparent on some echinoderm plates (Fig. 5H). Similar to facies 1, thin sections of facies 3 show visible mottled organic-rich and dispersed detrital-silt-rich domains suggesting that cryptobioturbation destroyed original sedimentary structures.

XRD analyses of two samples of facies 3 indicate that the matrix of facies 3 is composed almost entirely of calcite with only very small amounts of detrital illite (Fig. 7A). The high concentration of calcite-recrystallized or -replaced bioclastic and biogenic material in the grain fraction of this facies also contributes to a high average calcite content. On average, clay minerals, feldspars, silica, dolomite, pyrite, and other minerals account for less than 25% of facies 3.

Programmed pyrolysis results on 13 samples of facies 3 (Table 2) show TOC content ranging from 0.46 to 15.9 wt.% with an average of 2.67 wt.% (Fig. 8A). S2 values range from 0.12 to 106.32 mg HC/g rock with an average of 13.02 mg HC/g rock (Fig. 8B), and HI values show a range from 21 to 673 mg HC/g TOC with an average of 272 mg HC/g TOC (Fig. 8C). Kerogen types inferred from these geochemical proxies show a bimodal trend of terrigenous-dominated (Type III) and marine-dominated samples (Type II) (Fig. 9).

Facies 4: Calcareous Wackestone

Calcareous wackestone, facies 4, displays an outcrop expression similar to that of facies 2 in that it is resistant, tabular, and thin-bedded to thick-bedded (0.03–1.1 m) with a white weathering surface and sharp non-erosional bases. Similarly, beds are either discrete or amalgamated in packages and have a fizz response to hydrochloric acid. Rare continuous wavy nonparallel laminae and trace fossils are apparent in outcrop. This facies differs from facies 2 in that it contains a higher percentage of silt- to

←

FIG. 4.—Stratigraphic correlation of the Pilmatué and Avilé Member outcrops measured in this study. Shown from left to right at each locality is a lithologic log, interpreted depositional environment, normalized XRD log, and the stratigraphic position of thin section and programmed pyrolysis samples. The stratigraphic height of the El Portón source intervals are boxed in black and labeled. The contact between the Avilé and Agua de la Mula members is the datum horizon.

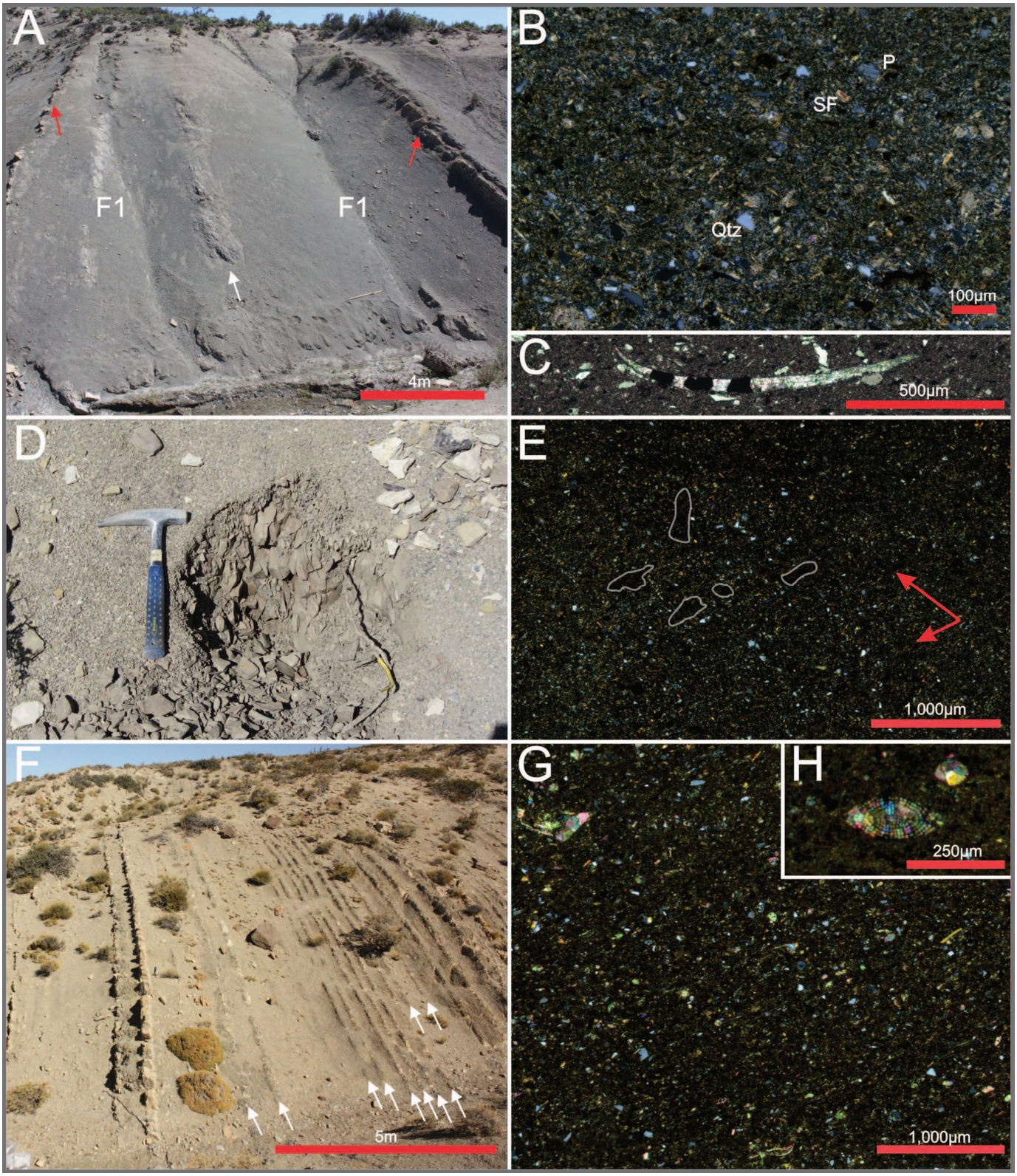

FIG. 5.—Examples of key features in facies 1 (Detrital-quartz-silt-bearing fine mudstone) and facies 3 (Detrital-quartz-silt- and shell-bearing fine mudstone). **A)** Outcrop view with facies 1 with a few isolated interbeds of facies 3 and facies 4. Scale bar is 4 m (~ 13 ft). **B)** Thin section of facies 1 with dispersed detrital-quartz-silt (Qtz), bladed shell fragments (SF), and rare plagioclase grains (P). **C)** Bivalve shell fragment recrystallized by blocky spar calcite cement. **D)** Outcrop view of the fissility of facies 1. Hammer is 33 cm (13 in). **E)** Thin section of facies 1 showing darker clotted organic-rich and lighter dispersed detrital-silt-rich domains. Several examples of the darker silt-free domains are outlined in white, and two uninterpreted examples are indicated with red arrows. **F)** Outcrop with facies 3 (marked by white arrows) interbedded with facies 1. **G)** Thin section of facies 3 showing higher concentration of thin shell fragments and lower concentrations of detrital quartz silt than seen in facies 1. **H)** Echinoderm plates in the center and radiolarian to the right recrystallized by sparry calcite cement and showing signs of compaction. The echinoderm plate shows evidence of a syntaxial overgrowth.

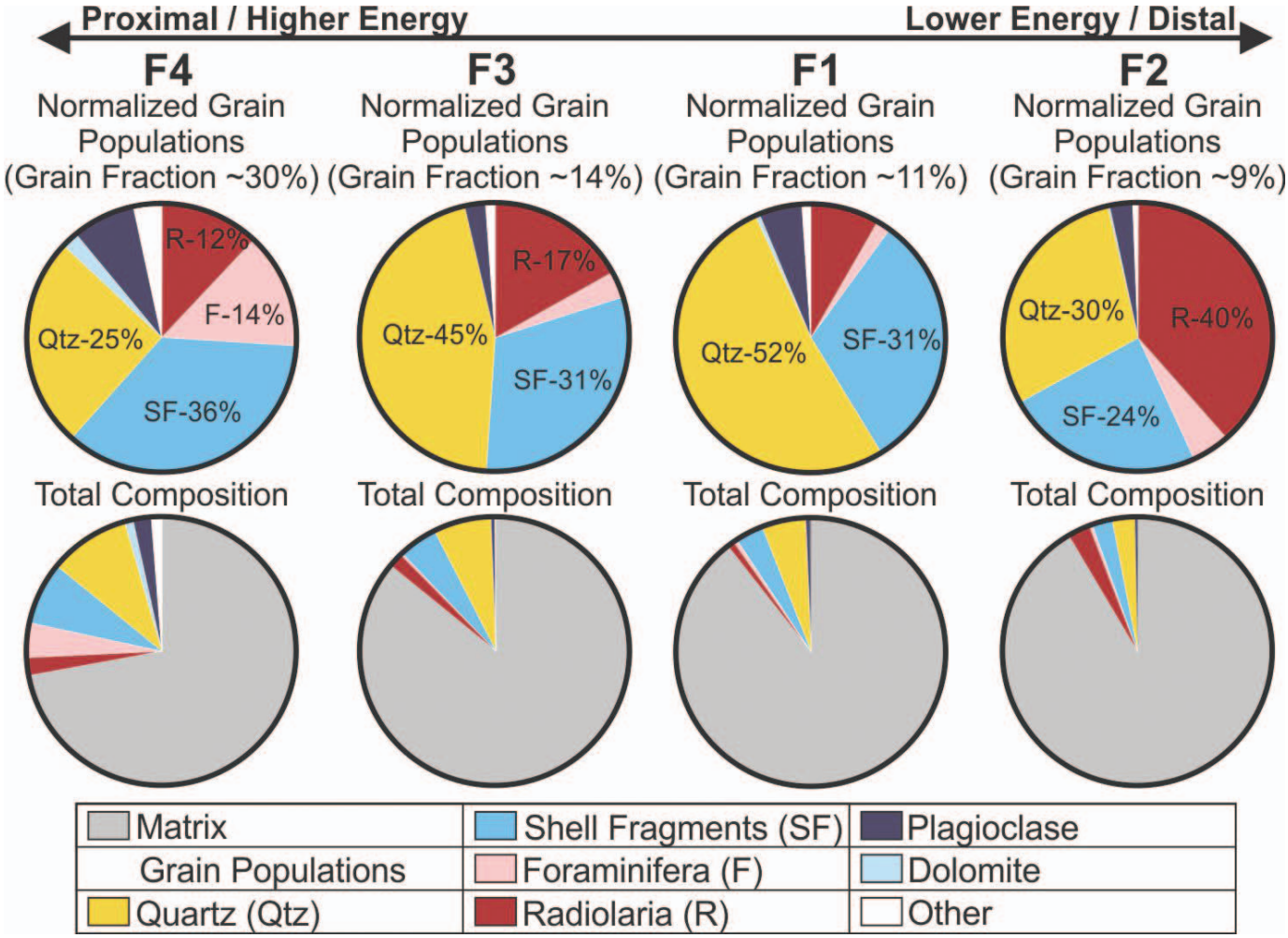

FIG. 6.—Proximal-to-distal trends by facies based on normalized grain populations and total compositions established through petrographic assessment of thin sections.

sand-size grains (≥ 15%); thus, it is categorized as a wackestone. Grains are composed mainly of reworked shell debris of variable size and/or disarticulated bivalves (Fig. 11A–D). Beds contain between 5 and 15% bioclastic material, and ammonite casts are common. Identifying specific taxa and genera is beyond the scope of this work but has been the focus of a number of other studies on the Agrio Formation (Aguirre-Urreta and Rawson 1997; Lazo 2004, 2006, 2007a, 2007b; Lazo et al. 2005, 2008). *Thalassinoides* and *Planolites* trace fossils were observed in outcrop in only one bed at the Puesto Chivito locality (Fig. 11E). Facies 4 constitutes an estimated 5% of the measured sections.

Though calcareous wackestone is dominated by micritic matrix in thin section (n = 5), the grain fraction accounts for ~ 30% on average. The grain fraction is dominated by sand- to silt-size shell material, consisting of bivalve, gastropod, ostracod, and unidentifiable fragments (Figs. 6, 11F–I). Most of the shell material is dispersed, but some larger shell fragments show parallel to subparallel alignment with the bedding plane (Fig. 11H). The grain fraction also contains medium-silt-size dispersed detrital quartz grains in quantities similar to those seen in facies 1, relatively high concentrations of medium-sand-size foraminifera, and minor Radiolaria, dolomite, feldspar, and pyrite. The foraminifera assemblage appears to be largely monotypic. All bioclastic and biogenic material has been recrystallized or replaced by drusy and/or blocky spar calcite cement. Some micritization is also visible (Fig. 11I). Similar to facies 2, intense bioturbation is inferred from the dispersed nature of the detrital silt in facies 4.

TABLE 2.—*Programmed pyrolysis data by facies with averages shown in bold.*

Facies	TOC (wt. %)	S2 (mg HC/g rock)	HI (mg HC/g TOC)	Kerogen Type
Facies 1 (n = 155)	0.31–10.66 (**1.57**)	0.04–70.28 (**3.44**)	6–709 (**153**)	Type I–Type IV
Facies 2 (n = 107)	0.25–3.8 (**1.20**)	0.06–21.29 (**3.97**)	14–637 (**262**)	Type I–Type IV
Facies 3 (n = 13)	0.46–15.9 (**2.67**)	0.12–106.32 (**13.02**)	21–673 (**272**)	Type I–Type IV
Facies 4 (n = 14)	0.54–4.14 (**1.77**)	1.42–24.73 (**8.86**)	261–682 (**474**)	Type I–Type II/III
Facies 5 (n = 2)	**1.66**	**8.73**	**526**	Type I

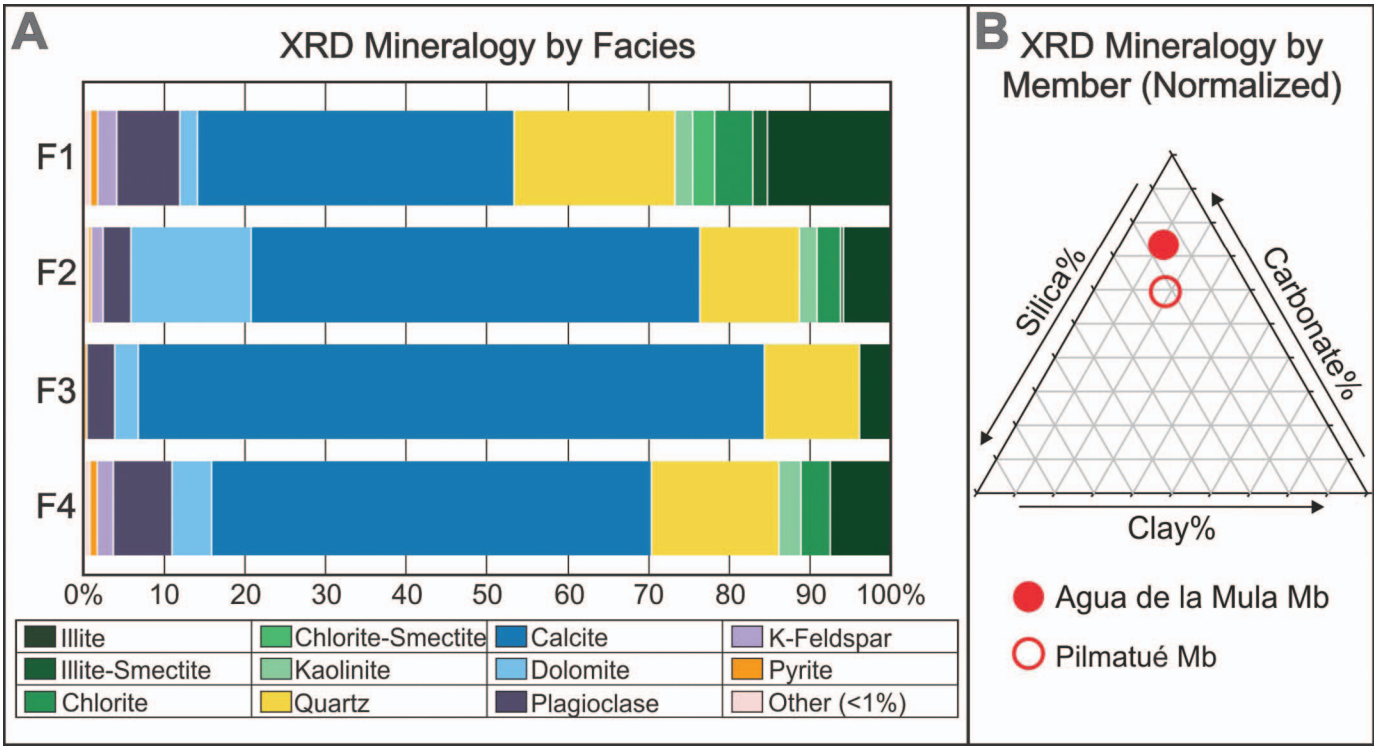

FIG. 7.—**A)** Mineralogy by facies based on X-ray diffraction. **B)** Composition of the upper Agua de la Mula Member and lower Pilmatué Member of the Agrio Formation based on X-ray diffraction values for normalized total quartz, total clay, and total carbonate.

XRD analyses on five samples of facies 4 indicate that the matrix of the facies is composed mainly of calcite with minor detrital clay-mineral composition, the most common of which is illite (Fig. 7A). Similar to facies 3, the high concentration of calcite-recrystallized or -replaced bioclastic and biogenic material in the grain fraction of facies 4 contributes to a high average calcite content. On average, clay minerals, feldspars, and silica account for around 40% of facies 4, which is dominated by ~ 55% calcite. Facies 4 contains minor amounts of dolomite, pyrite, and other accessory minerals.

Programmed pyrolysis results on 14 samples of facies 4 (Table 2) show TOC content ranging from 0.54 to 4.14 wt.% with an average of 1.77 wt.% TOC (Fig. 8A). S2 values range from 1.42 to 24.73 mg HC/g rock with an average of 8.86 mg HC/g rock (Fig. 8B), and HI values range from 261 to 682 mg HC/g TOC with an average of 474 mg HC/g TOC (Fig. 8C). Kerogen types inferred from these geochemical proxies are marine-dominated (Type II) to mixed terrigenous and marine (Type II/III) (Fig. 9).

Facies Interpretations: Proximal-to-Distal Trends

The main constituents of the four volumetrically most abundant facies of the Pilmatué and Agua de la Mula members in this distal part of the basin can be separated into three groups: detrital material, benthic and/or pelagic biogenic material, and carbonate mud (micrite). The mud-dominated nature of these facies indicates that they were likely deposited in a relatively low-energy environment, below storm wave base (Morris et al. 2006; Wilson and Schieber 2014; Schwarz et al. 2018) It is important to note that storm wave base may not represent one depth, but a range of depths dependent on storm strength (Peters and Loss 2012). The average depth of storm wave base in open-ramp systems is between 20 and 70 m, and the maximum water depth reported for the Early Cretaceous Neuquén embayment was ~ 200 m (Sagasti 2005; Immenhauser 2009). Therefore, the approximate water-depth range for these deposits is between ~ 50 and 200 m. Though rare storm events may have occurred during the deposition of these facies, the presence of pervasive cryptobioturbation in thin section, horizontal trace fossils in outcrop in facies 2 and 4, and a lack of scouring and other storm-deposit indicators (e.g., HCS) suggest that this system is generally characterized by lower-energy conditions (Burchette and Wright 1992; MacEachern et al. 2010). Though cryptobioturbation prevents the identification of sedimentary features in thin section, no outcrop observation in this field area, such as slumping or debris-flow deposits, were seen that indicate a departure from a homoclinal-ramp geometry. However, the exact nature and ramp angle through space and time requires additional focused evaluation and cannot be confidently determined based only on the data presented herein. Therefore, we defer to the low-gradient-ramp model well established in the literature (Legarreta and Gulisano 1989; Legarreta and Uliana 1991, 1999; Sagasti 2005; Lazo et al. 2005, 2008; Schwarz et al. 2011).

The detrital-material component consists of siliciclastic detrital silt (mainly quartz with minor plagioclase and K-feldspar), detrital argillaceous mud (clay), and reworked bioclastic shell material. This detrital material was largely transported offshore from a siliciclastic-dominated shoreline and could have been transported by either 1) hyperpycnal flows, 2) hypopycnal plumes, or 3) wave- and/or current-enhanced sediment-gravity-flow remobilization of siliciclastic and bioclastic shallow marine deposits (Bhattacharya and MacEachern 2009; Wilson and Schieber 2014; Denommee et al. 2016; Schieber 2016; Birgenheier et al. 2017). The shallow-ramp, low-angle-gradient model for the Early Cretaceous Neuquén Basin supports these three possible depositional mechanisms for detrital material (Schieber 2016). The highly fragmented nature of the bioclastic shell material indicates a long transport distance from more shore-proximal zones (Egenhoff and Fishman 2013) located roughly ~ 150 km south and

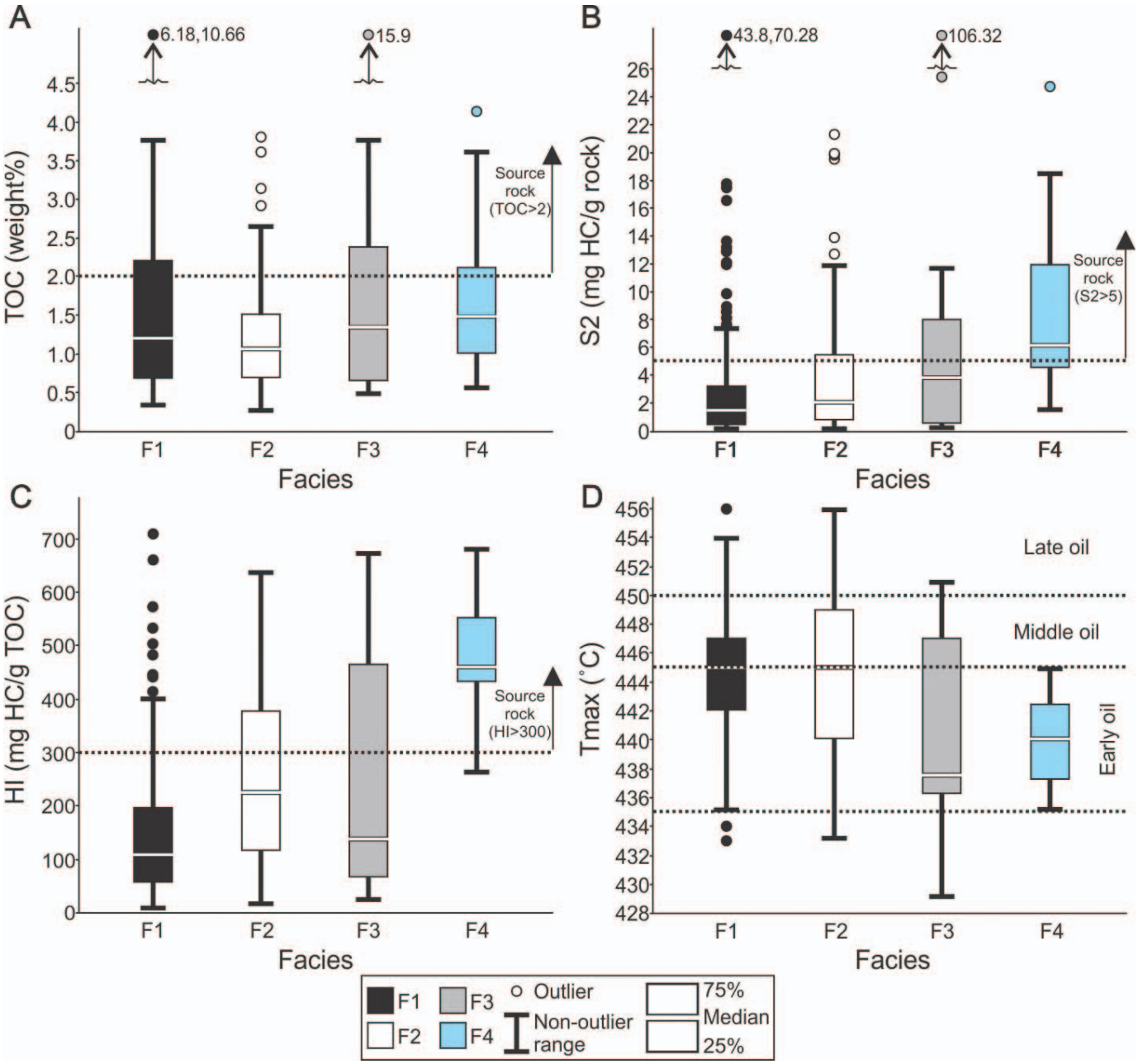

FIG. 8.—Variations in geochemical properties by facies based on programmed pyrolysis. Box plots show median, distribution quartile, non-outlier range, and outliers of each parameter.

~ 60 km east of these localities (Fig. 2), likely through the same mechanism responsible for the transport of the detrital silt and argillaceous mud. The shore-proximal zone to the east is mentioned because some of the shell material may have been sourced from the neritic carbonate factory along the eastern margin of the basin.

Benthic foraminifera indicate some benthic production of biogenic material with the possibility of further transport via traction currents (Egenhoff and Fishman 2013), which may be evident from the admixing of foraminifera with other bioclastic material seen in facies 3. The presence of Radiolaria indicates some pelagic production of biogenic material that was likely deposited by suspension settling. Possible sources for carbonate mud commonly described for Cretaceous marine systems are 1) pelagic calcareous nannofossils, 2) whitings, and/or 3) transported, shallow marine, benthic carbonate that has been disarticulated and reworked into mud, particularly from calcareous algae (Bathurst 1975; Bornemann et al. 2003).

Based on the processes indicated above, grain population trends within these facies can be utilized to establish relatively higher energy to relatively lower energy or shoreline proximal to distal depositional trends, respectively (Fig. 12). Facies 4 has the highest percentage of grains (versus matrix) at ~ 30%, and the dominant grain populations are shell fragments, principally macrofossils, and detrital quartz grains (Fig. 6). This relatively high percentage of macrofossils and detrital silt indicates that facies 4 was deposited under the highest-energy conditions and is likely the most proximal facies, with the highest input of detrital material transported from a siliciclastic-dominated shore-proximal zone (Fig. 12). The high

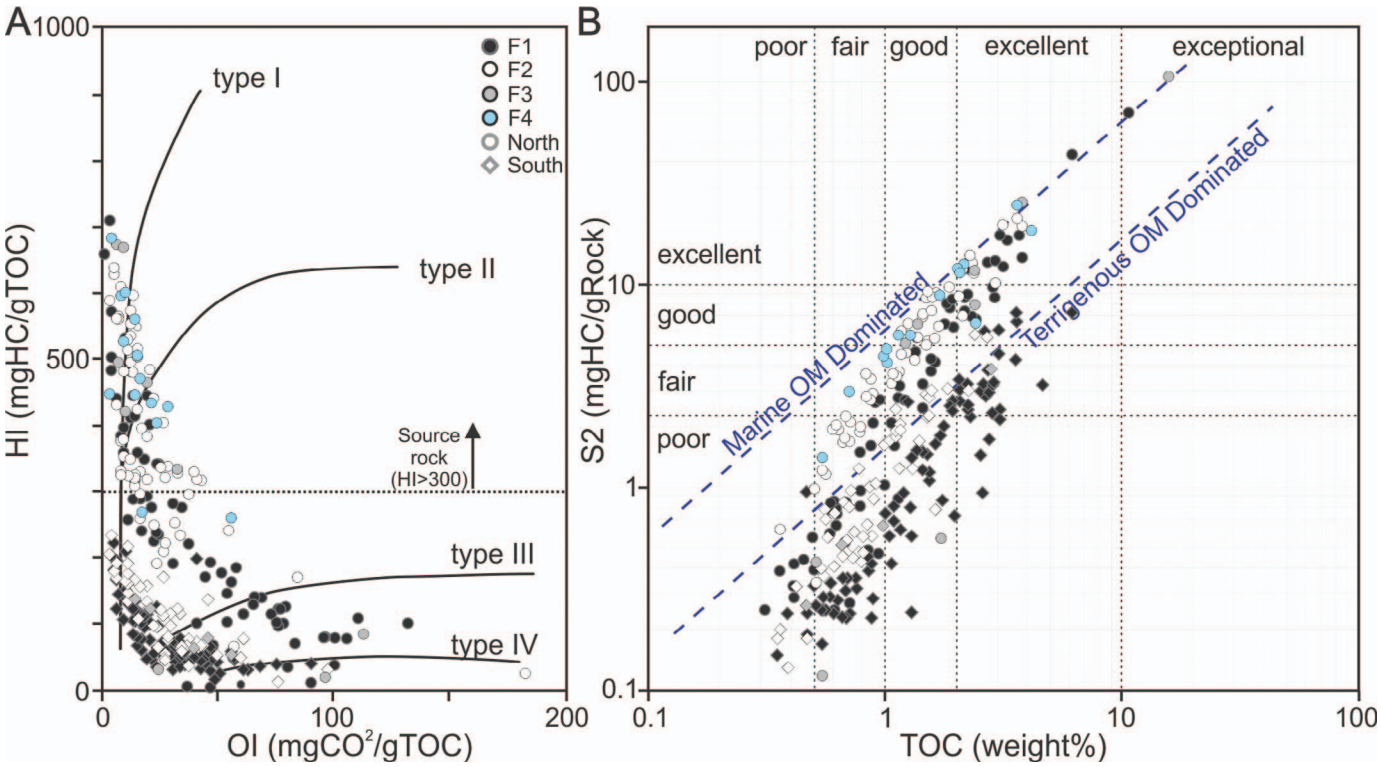

FIG. 9.—**A)** Hydrocarbon index versus oxygen index (pseudo–van Krevelen diagram). **B)** S2 versus total organic carbon (TOC). Trendlines represent HI values (marine, 600 HI; terrigenous, 150 HI) calculated from S2 and TOC. Both are colored by facies with shapes denoting location.

carbonate percentage compared to quartz and argillaceous clay minerals from XRD is a function of the high percentage of calcite derived from recrystallized or replaced macrofossil and microfossil bioclastic material and biogenic material, which dilutes the detrital-quartz and clay signal. Facies 3 displays XRD percentages and normalized grain population percentages similar to facies 4, yet with a markedly lower percentage of grains at ~ 14%, a dominance of microfossil shell fragments as opposed to macrofossils, and a lower abundance of benthic forams (Fig. 6). Therefore, facies 3 represents a slightly more distal, lower-energy environment than facies 4 (Fig. 12). Facies 1 contains slightly fewer grains than facies 4 and 3, at ~ 11%, with a marked shift in grain population from mixed bioclastic- and quartz-dominated to strongly quartz-dominated (Fig. 6). This is apparent in the XRD data, which display a relatively high percentage of detrital argillaceous clay minerals, and a calcite dilution of detrital components is lacking (Fig. 7). The relatively high percentage of detrital silt and detrital argillaceous mud in facies 1 (though lower absolute detrital-silt percentages than facies 4 and 3), along with a slightly lower microfossil abundance compared with facies 3, is interpreted as representing slightly more distal, lower-energy deposition than facies 3 (Fig. 12). Facies 2 has the lowest percentage of grains at 9%, the lowest absolute abundance of detrital quartz grains, and is dominated by pelagic Radiolaria (Fig. 6). As such, it is interpreted as representing the most distal or lowest-energy deposits (Fig. 12).

Based on the model for the distribution of grain populations presented here, it would be expected that Radiolaria would be more abundant in the distal facies than in the more proximal facies. This trend is clearly seen in the comparison of facies 1 and facies 2, but is less substantial when comparing facies 2 with facies 3 and 4 (Fig. 6). The similar overall high abundance of Radiolaria in the most proximal (facies 4) and most distal (facies 2) facies may have several explanations. From a depositional standpoint, this similarity in abundance may be a result of increased winnowing out of mud in the more proximal, high-energy zones leading to concentrations of Radiolaria. Conversely, this trend could indicate that radiolarian abundances do not follow proximal-to-distal trends as they are responding to other drivers, such as nutrient upwellings and/or silica supply. Alternately, Radiolaria abundance by facies may reflect not only production but also the preservation of Radiolaria, which may be affected by diagenesis inequality across facies types (Frank et al. 1999; Westphal et al. 2004). Finally, it should also be considered that the sample size for thin sections of facies 1 (n = 27) and facies 2 (n = 21) is more substantial and comparable with that of facies 3 (n = 8) and facies 4 (n = 5) due to their relative abundance in outcrop.

Facies 2 displays the highest ratio of marine-dominated organic matter to terrestrial organic matter (Fig. 9). Thus, the organic geochemical data support facies 2 as the most distal or low-energy facies with the lowest amount of dilution by hinterland-derived material. Similarly, facies 1, which is interpreted as more proximal or high energy with a higher detrital component compared with facies 2, displays a mixed terrestrial and marine organic matter signal or a biodegraded marine organic matter signal. Both of these signals would be prominent in more proximal settings prone to offshore transport of terrestrial material and conditions less conducive to the preservation of organic material (Fig. 9).

Rare Facies of the Pilmatué and Agua de la Mula Members

There are three facies (facies 5–7) in the distal ramp of the Pilmatué and Agua de la Mula members that are not volumetrically significant (Table 1). All beds of facies 5, calcareous intraclastic packstone, collectively account for only ~ 2 m of the ~ 1200 m measured. Facies 5 is interpreted as resulting from subaqueous erosion and redistribution of rapidly stabilized offshore to basinal carbonate mudstone deposits, possibly related to energetic transgressive events or ravinement surfaces. Facies 6, calcareous floatstone, is observed as only several centimeter-

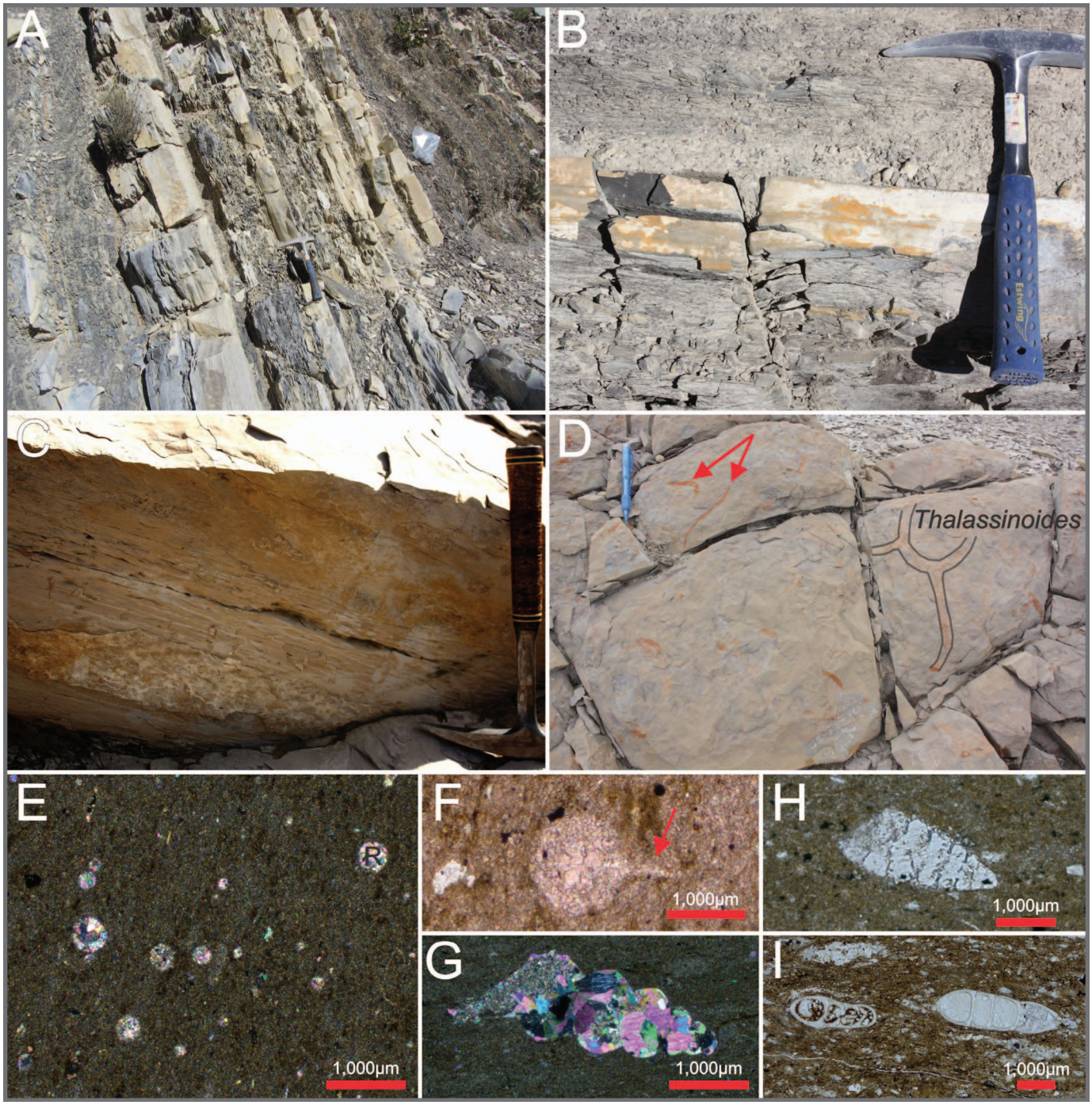

FIG. 10.—Examples of key features in facies 2 (Radiolarian-bearing fine mudstone). **A)** Outcrop with resistant facies 2 thinly interbedded with recessed facies 1. Both facies are laterally continuous. Hammer is 33 cm (13 in). **B)** Close-up of facies 2 showing the white weathering appearance. **C)** Facies 2 showing discontinuous, wavy, nonparallel laminae. **D)** Bedding plane of facies 2 with orange tuff-stained *Thalassinoides* trace fossils visible. One example is outlined and annotated and two uninterpreted examples are indicated with red arrows. Pencil is 14.5 cm (5.70 in). **E)** Thin section of facies 2 showing blocky-spar-calcite-replaced radiolarians (R). **F)** Sparry-calcite-replaced radiolarian with preserved spine (red arrow). **G)** Blocky-spar-calcite-recrystallized gastropod. **H**, **I)** Blocky-spar-calcite-recrystallized or -replaced benthic foraminifera with some of its original test morphology preserved (H, possibly agglutinated: I, possibly *Nodosaridae*).

thick beds in the upper part of the Pilmatué Member at Puesto Chivito. Facies 6 is interpreted as representative of isolated and localized bioherms, due to their rarity, lack of lateral continuity and lenticular shape, and the nature and positioning of the included bioclastic material. Facies 7, tuff, though less volumetrically limited than facies 5 and 6, is interpreted as distal ash-fall deposits from the active magmatic arc to the west. A lack of sedimentary structures in deposits of facies 7 indicate these deposits likely settled out of suspension.

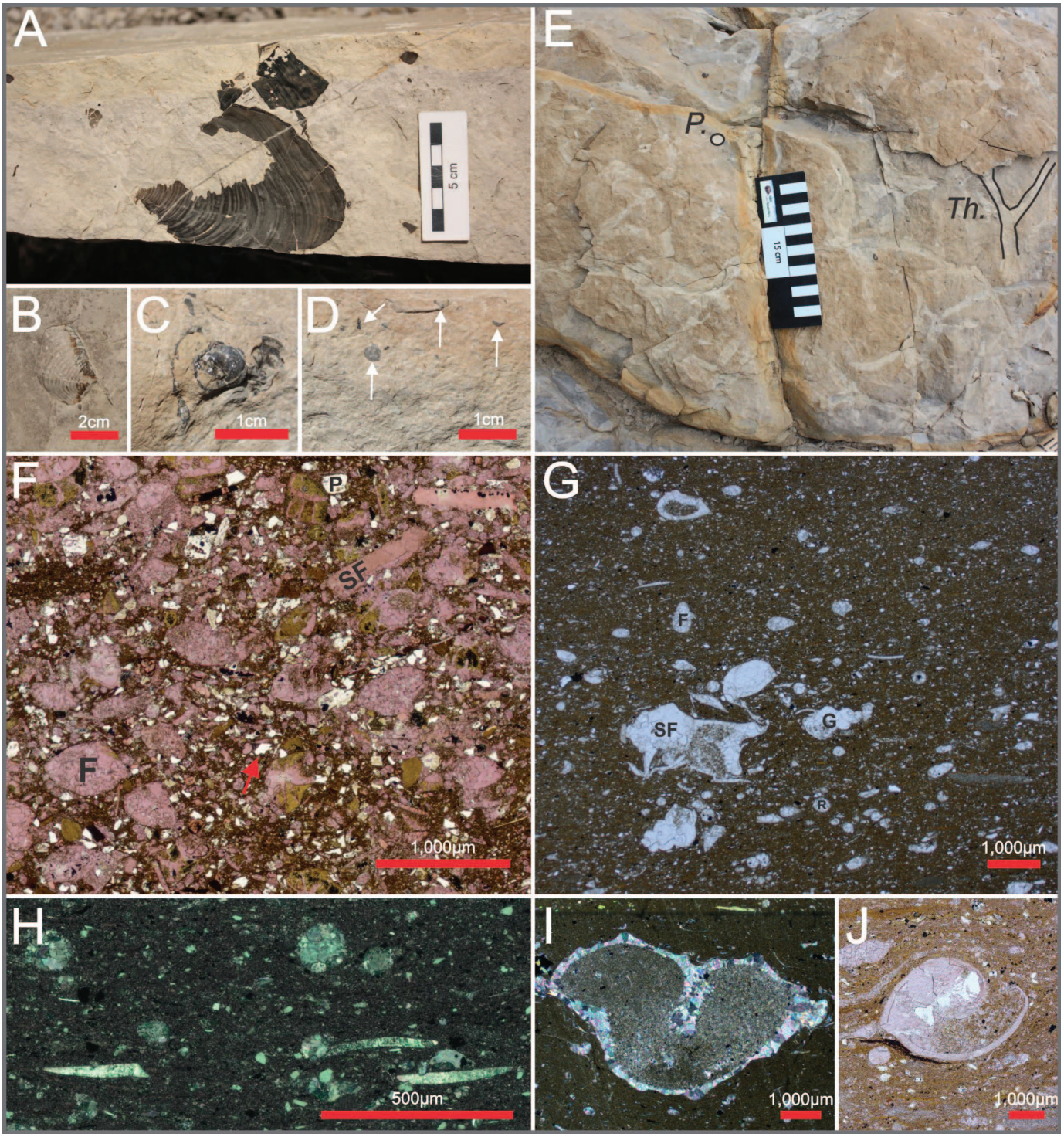

FIG. 11.—Examples of key feature in facies 4 (Calcareous wackestone). **A)** Outcrop with facies 4 showing a large bivalve shell, **B)** a cast of an articulated bivalve, **C)** a gastropod fragment, **D)** millimeter-scale dispersed shell fragments (white arrows), and **E)** abundant *Thalassinoides* and rare *Planolites* trace fossils visible on top of bedding plane. One example of each is annotated. **F)** Dual carbonate-stained thin section showing wackestone with *Epistomina* benthic foraminifera (F), shell fragments (SF), detrital-quartz-silt (red arrow), and plagioclase crystals (P). **G)** Thin section showing a wackestone with shell fragments (SF), gastropods (G), forams (F), (possibly agglutinated), and Radiolaria (R). **H)** Thin section showing wackestone displaying blocky-spar-calcite-recrystallized shell fragments oriented subparallel to lamination. Replaced Radiolaria are visible. **I)** Blocky-spar-calcite-recrystallized articulated shell; note micrite in the cell center. **J)** A slightly compressed, calcite-recrystallized ostracod.

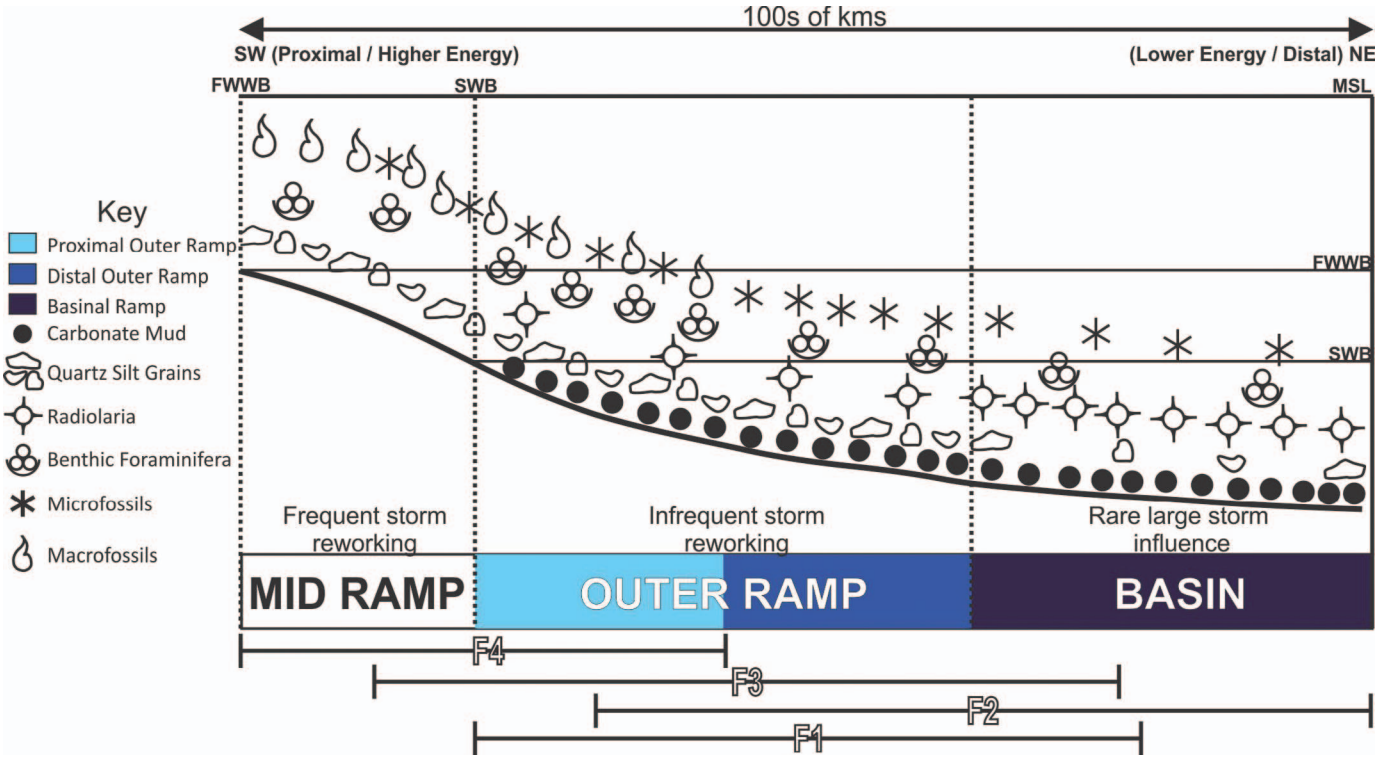

FIG. 12.—Summary schematic diagram showing the distribution of grain populations across the distal part of a carbonate ramp with interpreted ranges of facies denoted. Interpreted depositional sub-environments from the sections measured in this study are shown. Adapted from Burchette and Wright (1992).

SOURCE POTENTIAL

The main programmed pyrolysis proxies of interest for evaluating source potential and thermal maturity in this assessment are TOC, S2, HI, OI, and Tmax. The programmed pyrolysis data from the measured sections in this study allow a comparison of source potential by facies as well as by locality and stratigraphic interval. This makes possible a south (paleo-updip and proximal) to north (paleo-downdip and distal) proxy comparison in the Pilmatué Member, as well as a proxy understanding of the Agua de la Mula Member in the north only (Figs. 1C, 4).

For several reasons, an evaluation of source potential by facies will focus on facies 1 and 2 only. First, these are the most volumetrically abundant facies by a significant margin (Appendices A, B, C). As such, they are the only facies with a statistically significant number of programmed pyrolysis data points (Table 2). Additionally, these facies are most relevant and comparable with previous literature concerning the source potential of the Agrio, with facies 1 equivalents ("black shale") typically described as the main organic-matter-bearing facies (Cruz et al. 1996; Tyson et al. 2005). Contrary to this assumption, geochemical analysis of programmed pyrolysis data indicates facies 1, on average, is only slightly TOC enriched (avg. 1.57 wt.%) relative to facies 2 (avg. 1.2 wt.%), and S2 values indicate that facies 2 (avg. 3.97 mg HC/g rock) has a slightly higher source quality than facies 1 (avg. 3.44 mg HC/g rock). Overall, there is a high degree of heterogeneity associated with the source of organic material in these samples, particularly for facies 1 and 2, with HI and OI trends plotting largely along Type II and mixed Type II–III trends (Fig. 9A). Perhaps most significantly, facies 2 displays more marine-dominated trends in organic matter than the more mixed terrigenous and marine trends of facies 1 (Fig. 9B). This indicates that facies 2 may be more oil prone in general than facies 1. Because of this weak relationship between source potential and facies, with both of the dominant facies acting as potential source units, identification of source intervals herein focuses on identifying temporally or stratigraphically significant intervals.

In this study, high source potential is defined as samples that display the following geochemical characteristics: TOC $\geq$ 2 wt.%, S2 $\geq$ 5 mg HC/g rock, and HI $\geq$ 300 mg HC/g TOC (Peters 1986; Peters and Cassa 1994; Pepper and Corvi 1995a, 1995b). Both northern and southern localities display samples that meet the established TOC and S2 value criteria for high source potential (Table 3; Fig. 13A, B). However, HI values are low throughout the southern localities (Table 3; Fig. 13C) with no southern samples meeting the established HI value criteria. HI values and geochemical diagrams of the data indicate the northern locality, El Portón, is dominated by marine to mixed terrigenous and marine organic material, whereas the southern localities, Puerta Curaco and Puesto Chivito, are dominated by terrigenous to inert organic material (Figs. 9, 13C). Tmax values indicate that the Pilmatué Member ranges from early oil to peak oil maturity in the north and from peak oil to late oil maturity at the southern localities (Fig. 13D). The Agua de la Mula in the north ranges largely from immature to early oil mature (Fig. 13D).

Based on stratigraphic clustering of samples reaching the above-established geochemical cutoffs, five source intervals have been established in the Aqua de la Mula and Pilmatué members at the northern El Portón locality (Table 4). Source interval one (SI1) is positioned in the basal section of the Pilmatué Member and has a thickness of $\sim$ 30 m (Figs. 4, 14). Source interval two (SI2) is positioned in the lower half of the Pilmatué Member and has a thickness of $\sim$ 25 m (Figs. 4, 14). Source interval 3 (SI3) is isolated to the upper section of the Pilmatué Member and is $\sim$ 20 m thick (Figs. 4, 14). Source intervals 4 and 5 (SI4, SI5) are located in the Agua de la Mula Member and are $\sim$ 7 m and $\sim$ 50 m thick, respectively (Fig. 15).

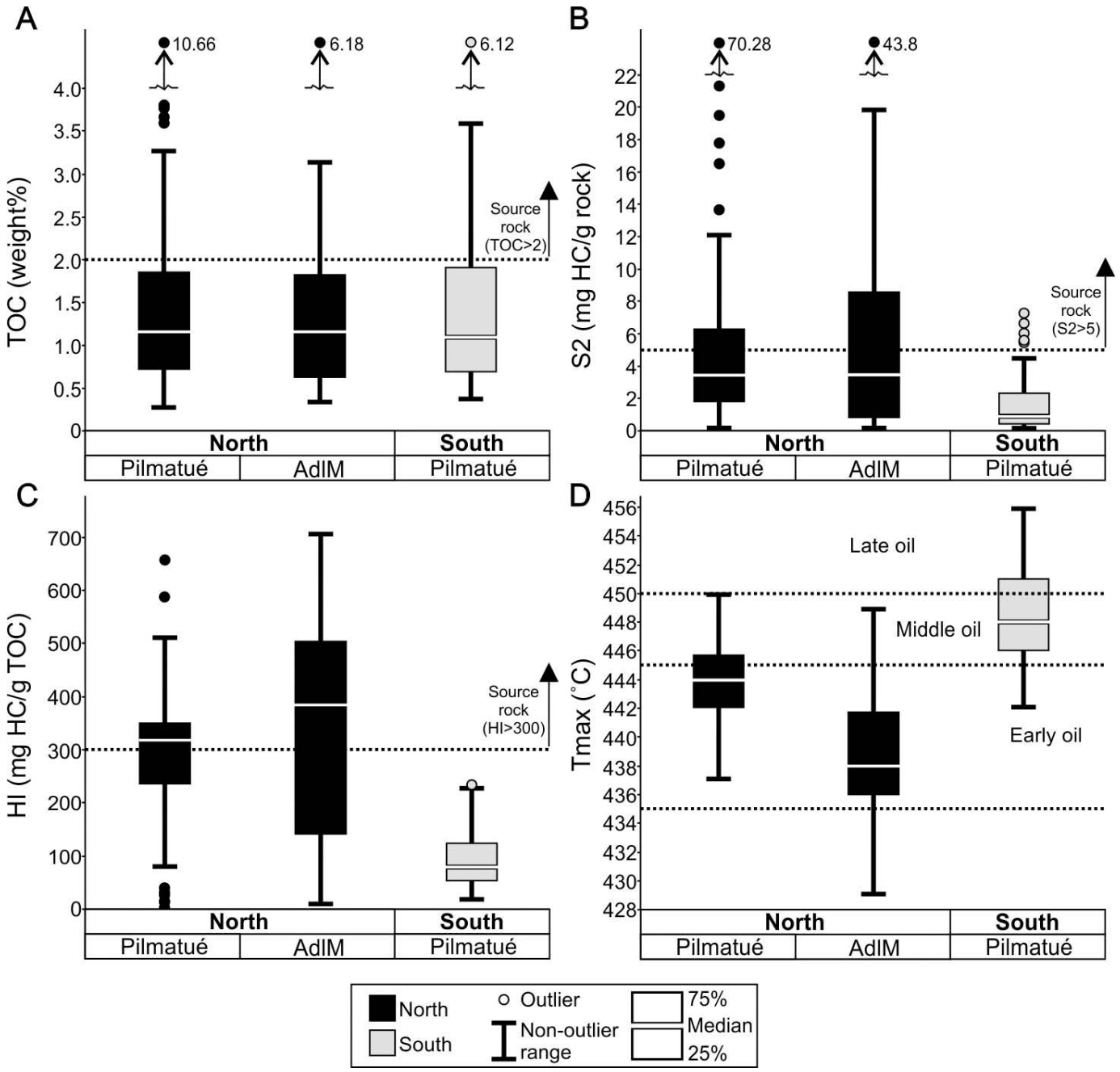

FIG. 13.—Variations in geochemical properties by location and member based on programmed pyrolysis. Box plots show median, distribution quartile, non-outlier range, and outliers of each parameter.

DISCUSSION

Depositional Mechanisms

Facies 1 through 4 of the Pilmatué and Agua de la Mula members are dominated by calcareous micrite by more than 84% on average (Figs. 6, 7), making for a thick accumulation (~ 600 m) of interbedded carbonate mudstone deposits. The interpretation that most of the Pilmatué and Agua de la Mula members deposited below storm wave base is consistent with the placement of storm wave base in a paleo-updip study conducted by Schwarz et al. (2018). Previous depositional models of the Agrio Formation have called upon suspension settling of mud as the dominant, if not sole, depositional mechanism below storm wave base (Sagasti 2005; Veiga and Schwarz 2017; Schwarz et al. 2018). One marked exception is the work of Comerio et al. (2018), which highlights evidence of current-influenced sedimentation in the basal part of the Aqua de la Mula member in deposits south of this study. Our detailed study of the mudstone-dominated facies of the Agrio Formation indicates the sub-storm-wave-base system was much more dynamic than simple suspension settling throughout the deposition of the unit.

The percentage of diagenetic versus depositional micrite or carbonate mud was not quantified as part of this study. A full detailed diagenetic study of the carbonate mudstone-dominated facies in the Agrio Formation, defined systematically here, is needed to truly isolate depositional micrite from diagenetic overprinting. With that caveat, we propose that interpreted

TABLE 3.—*Programmed pyrolysis data by area and member with averages shown in bold.*

Area	Member	TOC (w.t %)	S2 (mg HC/g rock)	HI (mg HC/g TOC)
North	Agua de la Mula (n = 97)	0.31–15.9 (**1.56**)	0.04–106.32 (**7.14**)	6–709 (**339**)
	Pilmatué (n = 55)	0.25–10.66 (**1.69**)	0.05–70.28 (**6.38**)	7–695 (**289**)
South	Pilmatué (n = 137)	0.35–6.12 (**1.37**)	0.06–7.30 (**1.52**)	14–234 (**96**)

depositional mechanisms for each facies below that should be further tested with cathodoluminescence (CL) and scanning electron microscopy (SEM) techniques to highlight diagenetic features.

Distinct features in facies 1–4 collectively can be explained by three main depositional mechanisms: 1) wave- and/or current-enhanced gravity flows delivering siliciclastic fluvial, and siliciclastic and bioclastic shallow marine sediments from areas paleodepositionally updip (Veiga and Schwarz 2017; Schwarz et al. 2018) to the offshore realm, 2) along-shore and oblique shallow water bottom-current-transported carbonate mud, sourced from the shallow marine carbonate-factory part of the shoreline, and 3) production of benthic and pelagic tests, both calcareous and siliceous (i.e., nannofossil and microfossils) (Fig. 16).

Wave- and/or Current-Enhanced Sediment Gravity Flows.—There are three possible depositional mechanisms that could be responsible for transporting fine-grained siliciclastic detrital silt (mainly quartz with minor plagioclase and K-feldspar), detrital argillaceous mud, and reworked bioclastic material offshore in this system: hyperpycnal flows, hypopycnal plumes, and wave- and/or current-enhanced sediment gravity flows (Bhattacharya and MacEachern 2009; Wilson and Schieber 2014; Denommee et al. 2016; Schieber 2016; Birgenheier et al. 2017). Though these sedimentary processes are typically distinguished using characteristic sedimentary structures, cryptobioturbation obliterated these in the Agrio Formation, preventing a definitive interpretation in this way. However, through the established understanding of the paleogeography of the Neuquén Basin, namely distance from the shoreline and estimated slope angles, we interpret that wave- and/or current-enhanced sediment gravity flows were responsible for transporting fine-grained detrital material offshore. Units in this study were deposited between $\sim$ 20 and $\sim$ 60 km from the nearest sandstone shallow marine shoreface deposits, which were dominated by longshore drift, but were at least $\sim$ 150 km away from the southern fluvial–deltaic point source that could have produced hyperpycnal flows and hypopycnal plumes (Sagasti 2005; Wilson and Schieber 2014; Schwarz et al. 2018). Additionally, previous works indicate slope angles in the inner ramp to middle ramp ranging from 0.1 to 0.01 degrees for the Neuquén Basin during deposition of the Agrio Formation (Hampson 2000; Sagasti 2005). Wave- and/or current-enhanced sediment gravity flows are the only documented process capable of transporting detrital silt over 150 km from the deltaic-dominated shoreline, particularly at this low slope angle (Schieber 2016) (Fig. 16). The slope gradient was likely too low for turbidity currents to be initiated through slope failure (Schieber 2016).

Though several offshore marine depositional models infer detrital-quartz-silt sourced from eolian or volcanic input (Werne et al. 2002; Sageman et al. 2003; Gabbott et al. 2010; Egenhoff and Fishman 2013), evidence in the four facies presented in detail herein do not support these interpretations. The dominance of subangular grains, rather than euhedral quartz grains, suggests that volcanic input is unlikely. Additionally, previous studies of altered tuffs in the Agrio Formation indicate that they consist primarily of volcanic glass shards with very little quartz and plagioclase present (Aguirre-Urreta et al. 2015, 2017; Schwarz et al. 2016). Eolian input is also unlikely because it fails to account for the transport of the detrital argillaceous mud, since flocculated clay particles cohesively form and act like silt- or sand-size particles that generally are not transported by wind (Nichols 2009; Schieber and Yawar 2009). The cohesive behavior of mud-size particles over a wide range of compositional variations and experimental conditions is well established (e.g., Schieber et al. 2007; Aplin and Macquaker 2011). Additionally, updip siliciclastic shoreface and offshore deposits documented by Schwarz et al. (2018) favor a siliciclastic shoreline over an eolian origin, inasmuch as there is no documentation of updip eolian deposits.

Oxygenation and the Preservation of Organic Matter.—It has been suggested that in shallow ($\leq$ 300 m), ancient epeiric seas, the development of seasonal thermal stratification related to dysoxic to anoxic periods would be likely, particularly under greenhouse conditions such as those that characterize the Early Cretaceous (Tyson and Pearson 1991; Sageman et al. 2003). *Thalassinoides* traces and cryptobioturbation occur in environments with oxygen levels ranging from dysoxic to oxic and suboxic to oxic, respectively. The presence of *Thalassinoides* burrows seen in outcrop and cryptobioturbation seen in thin section suggests that oxygenated to suboxic conditions existed at the sediment–water interface during the deposition of the Agrio Formation. Therefore, sedimentologic lines of evidence do not support prolonged anoxic periods of deposition. Yet, clearly, a subset of samples preserves a high amount of organic material (Fig. 8). Most established geochemical models would assert that this defined subset of samples preserves evidence of anoxic conditions to promote the preservation of organic matter and deter biodegradation (Demaison and Moore 1980; Pedersen and Calvert 1990; Ingall et al. 1993; Calvert et al. 1996; Tyson 2001; Van Dongen et al. 2006). However, the preservation of organic material in an oxygenated water column may also be explained by optimal rates of production, destruction, or dilution. For example, the encapsulation of organic matter into "marine snow" created local pore-water anoxia in the algal masses (Bohacs et al. 2005; Macquaker et al. 2010b) that reached the sea floor during periods of relative calm when weak bottom currents slightly buried and preserved it (Comerio et al. 2018; Minisini et al. 2018). Furthermore, the preservation of organic material

TABLE 4.—*Programmed pyrolysis data of the El Portón source intervals.*

Member	Source Interval	Stratigraphic Height (m)	Stratigraphic Thickness (m)	TOC (wt. %)	S2 (mg HC/g rock)	HI (mg HC/g TOC)
Agua de la Mula	5 (n = 29)	415–465	50	0.54–6.18 (**2.05**)	1.02–43.80 (**10.20**)	102–709 (**448**)
	4 (n = 6)	350–357	7	1.55–15.9 (**4.52**)	4.32–106.32 (**27.95**)	276–668 (**537**)
Pilmatué	3 (n = 4)	260–285	25	2.39–3.61 (**2.86**)	5.92–21.29 (**11.97**)	216–588 (**402**)
	2 (n = 32)	105–130	25	0.51–17.22 (**2.96**)	0.56–82.29 (**12.59**)	32–659 (**344**)
	1 (n = 7)	30–62	32	2.12–4.14 (**2.93**)	3.80–18.56 (**9.70**)	175–114 (**316**)

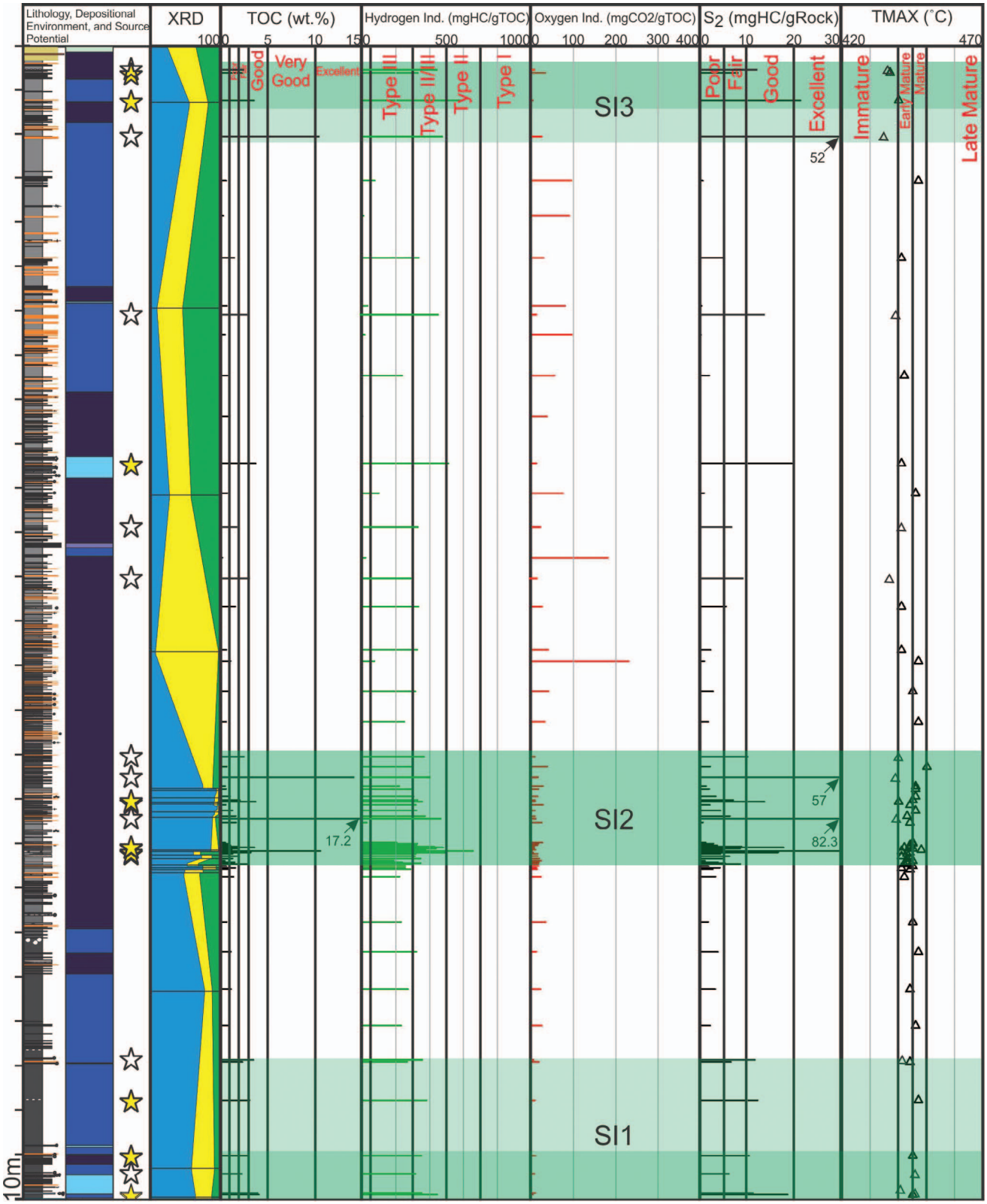

FIG. 14.—Log data for the Pilmatué Member at the northern El Portón locality including lithology, interpreted depositional environment, and XRD and programmed pyrolysis data. Samples with source potential are marked with a star. Yellow stars are for samples for which stratigraphic height is precisely known, and white stars are for samples for which approximate stratigraphic height is known. The stratigraphic height of individual XRD samples is marked by a black horizontal line in the XRD track. Priority source intervals are numbered and highlighted in green, with the darker green representing conservative thickness and the lighter green representing liberal thickness. See Figure 4 for lithologic, depositional environment, and XRD key.

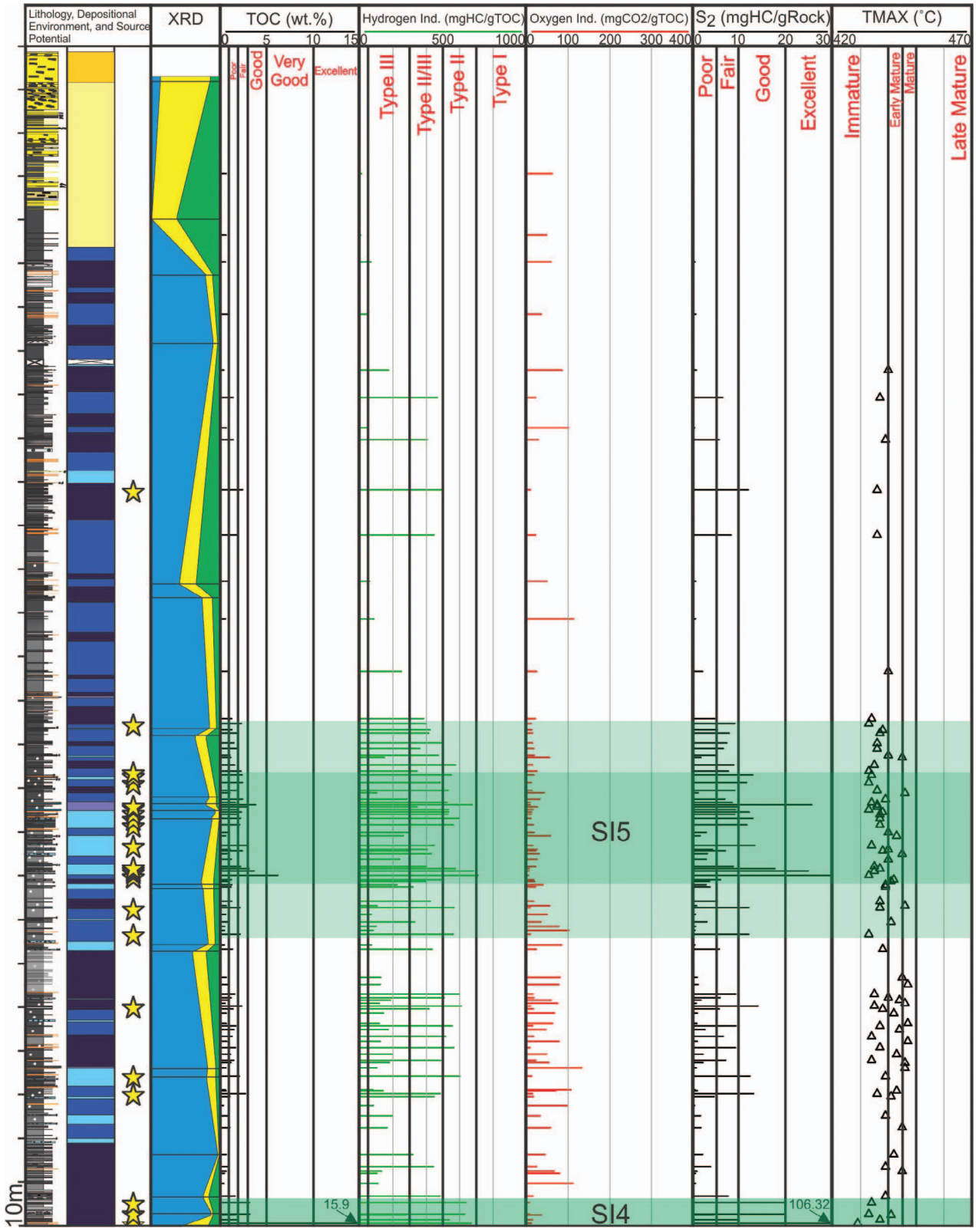

FIG. 15.—Log data for the Agua de la Mula Member at the northern El Portón locality including lithology, interpreted depositional environment, and XRD and programmed pyrolysis data. Samples with source potential are marked with a star. Yellow stars are for samples for which stratigraphic height is precisely known, and white stars are for samples for which approximate stratigraphic height is known. The stratigraphic height of individual XRD samples is marked by a black horizontal line in the XRD track. Priority source intervals are numbered and highlighted in green, with the darker green representing conservative thickness and the lighter green representing liberal thickness. See Figure 4 for lithologic, depositional environment, and XRD key.

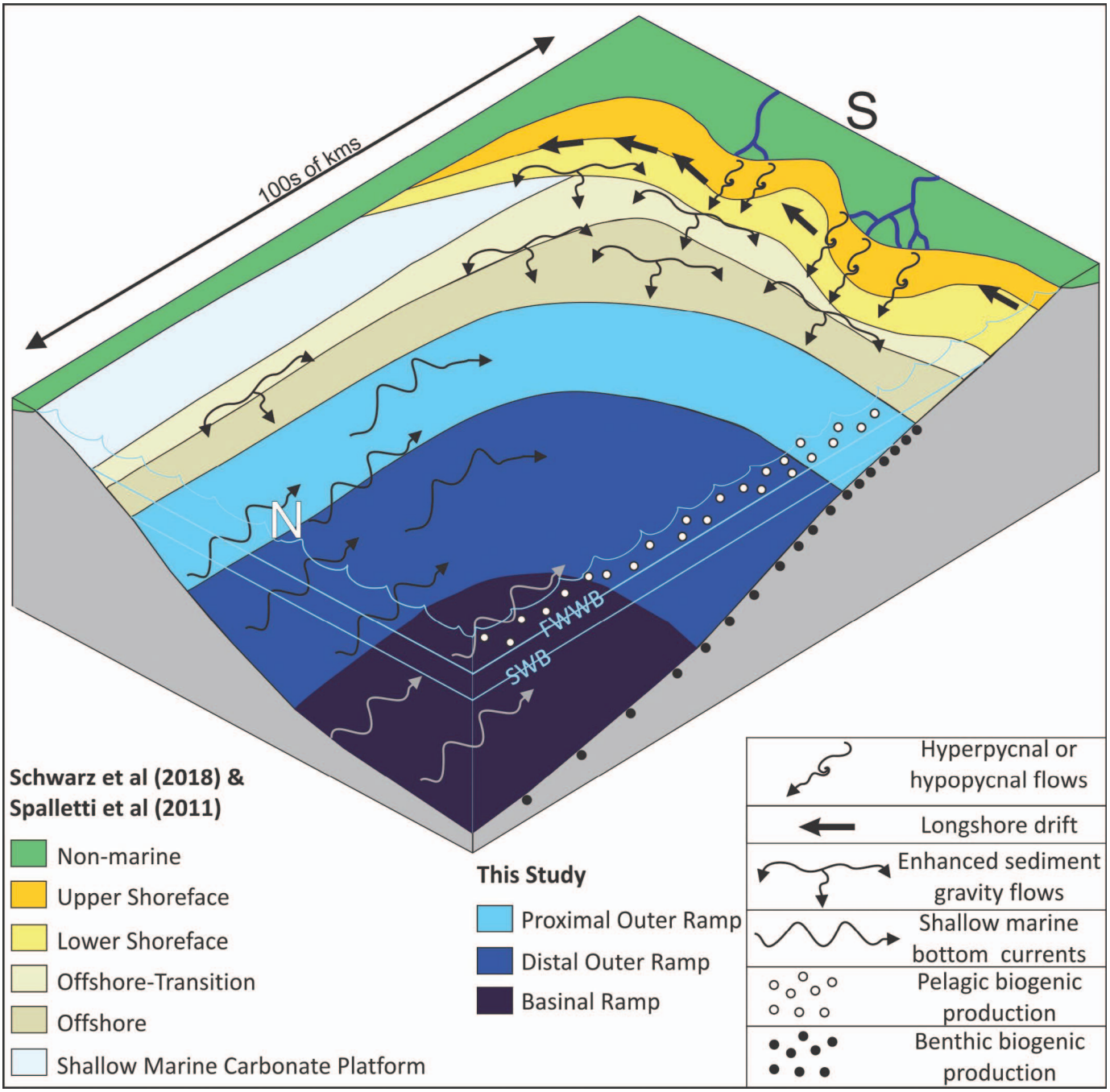

FIG. 16.—Schematic illustration of interpreted distal environments of deposition from the sections measured in this study, with depositional mechanisms outlined. The southern siliciclastic shoreline is modified from Schwarz et al. (2018), and the northern carbonate and siliciclastic shoreline is modified from Spalletti et al. (2011).

within an oxygenated sediment–water interface zone that supports burrowing infauna can be explained by rapid deposition of the marine snow when planktonic blooms outpaced the rate of organic-carbon decay (Macquaker et al. 2010b). Future work on the inorganic geochemistry of redox-sensitive elements (e.g., Mo, V, Cu, Co) should be conducted to support these sedimentological findings.

Origin of Carbonate Mud.—Models of deep marine Cretaceous systems typically assert that the bulk of carbonate mud or micrite is composed of calcareous nannofossils that lived in the water column and then settled to the sea floor (Bornemann et al. 2003; Sonnenberg 2011; Eldrett et al. 2015; Fairbanks et al. 2016). Though a number of studies have identified nannofossils in the Agrio Formation, chiefly for biostratigraphic assessments, no study has attempted to quantify what percentage of a given sample they account for (Aguirre-Urreta et al. 1999, 2005, 2017; Comerio et al. 2018). Slide-smear analyses reveal that the matrix contains rare, barely identifiable nannofossil tests of the most dissolution-resistant Cretaceous nannofossil species *Watznaueria barnesiae* (Fig. 17), but severe burial and weathering diagenesis makes quantifying the original volume of nannofossils present impossible (David Watkins, personal

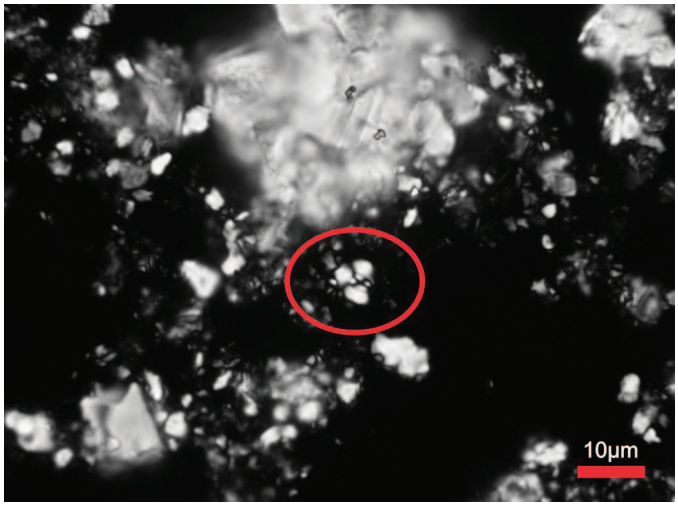

FIG. 17.—Smear slide of facies 2 showing a *Watznaueria barnesiae* calcareous nannofossil exhibiting advanced diagenetic alteration including breakage (red circle).

communication 2018). An average of sedimentation rates established and compiled by Locklair et al. (2011) for Cretaceous marine chalk deposits in pelagic environments indicates a sedimentation rate of 1.84 cm/ky (ranging from 1.1 to 3.5 cm/ky), suggesting that nannofossil sedimentation rates would be of a similar magnitude. Approximate sedimentation rates, based on extensive biostratigraphic studies and available U-Pb age dates, indicate a sediment accumulation rate of 8.93 cm/ky for the Agua de la Mula Member and an average sediment accumulation rate of 7.17 cm/ky for the Pilmatué Member in this part of the basin (Martinez et al. 2012, 2015, Aguirre-Urreta et al. 2015, 2017; Schwarz et al. 2016). Because the sediment accumulation rates in the distal part of the Agrio Formation are almost an order of magnitude greater than those explained by nannofossil accumulation alone, and because the dominant component of the facies is carbonate mud, we propose the hypothesis that there was likely an additional depositional source and a depositional mechanism besides pelagic settling of carbonate mud alone. This hypothesis should be further tested from other localities and with more detailed diagenetic studies that quantify the percentage of diagenetic versus depositional micrite.

Additional micritic carbonate may have been derived from siliciclastic-poor, shallow carbonate-rich regions of the shoreline, where the fine-grained fraction was winnowed out of shallow carbonate periplatform sediment, transported laterally and obliquely, and deposited offshore as a drift (Betzler et al. 2013, 2014; Eberli and Betzler 2019). Existing paleogeographic reconstructions document a siliciclastic shoreline to the south and a shallow carbonate platform, or neritic carbonate factory in the context of a ramp system, to the east and northeast (Spalletti et al. 2011; Schwarz et al. 2018). Carbonate platform environments produce large amounts of mud-size grains through varying degrees of mechanical degradation of skeletal material (e.g., calcareous green algae), bioerosion, and chemical and/or biochemical precipitation (Neumann and Land 1975; Gischler and Zingeler 2002; Betzler et al. 2013). As such, we propose neritic-carbonate-factory-derived mud may have been transported offshore and deposited along and oblique to the shoreline by offshore to oblique-to-shore bottom currents (Figs. 2, 16). One possible bottom-current mechanism is contour currents that originated from paleoceanographic circulation patterns driven by a combination of thermohaline- and wind-driven currents (Stow et al. 2002; Frébourg et al. 2016). These currents would likely have been modified by interaction with the seafloor topography and deflected clock-wise offshore by the Coriolis force. These inferred shallow-water contour currents may have formed a shoreline-parallel carbonate mudbelt. The range of sediment accumulation rates associated with carbonate-factory marginal environments, ~ 4–30 cm/ky, are more in line with the magnitude of sediment accumulation calculated for the measured sections in this study (McNeill 2005; Lokier and Steuber 2008; Phelps et al. 2015). Thus, a combination of pelagic nannofossil production and shallow-water bottom currents accounts for the carbonate mud in the Agrio system, inasmuch as nannofossil test production alone is unlikely to account for the documented high sedimentation rates (Fig. 16). A higher component of shallow platform-derived micrite than pelagic calcareous production has been briefly suggested by Sagasti (2005) and is further supported by accumulation rates presented here.

Benthic and Pelagic Deposition.—Benthic biogenic production in this system resulted in the deposition of benthic foraminifera (Fig. 16). Where concentrations of these benthic forams in the succession are high and rather monotypic, such as high concentrations of *Epistomina* in facies 4, they represent a local population, with limited secondary transport (Sagasti and Ballent 2002). Since other lines of evidence suggest that active currents characterized the system, where the foraminifera assemblages are more mixed and are admixed with other transported shell material, such as seen in facies 3, microfossils may have experienced entrainment, transport in active currents, and subsequent redeposition. Pelagic biogenic calcareous-test and silica-test production in this system resulted in the deposition of calcareous nannofossils and dispersed Radiolaria through suspension settling (Fig. 16). Note that Radiolaria tests that were originally siliceous have been dissolved and replaced with blocky spar calcite cement, a significant diagenetic event. The lack of preservation of nannofossil tests also indicated extensive diagenesis.

Facies Assemblages and Depositional Environments

The relative influence of each of the three depositional mechanisms outlined above in each facies indicates depositional sub-environments in the distal offshore realm of a mixed siliciclastic to carbonate ramp. Facies stack stratigraphically into facies assemblages that record deposition in one sub-environment. We propose that this part of the ramp, which was previously characterized as simply basinal, is divided into the following three depositional sub-environments: basinal ramp, distal outer ramp, and proximal outer ramp (Table 5; Figs. 12, 16, 18). The vertical stacking pattern of these depositional sub-environments has been established for each outcrop locality (Fig. 4). This depositional model should be further tested in other localities.

Basinal Ramp (FA1).—This facies assemblage is dominated by packages of facies 2 (radiolarian-bearing fMs) interbedded with volumetrically minor amounts of facies 1 and 3 (Table 5; Fig. 18). The environment is dominated by micrite, derived from the likely combination of pelagic nannofossils with shallow-water bottom-current-transported carbonate sourced from the northeastern carbonate factory (Figs. 2, 16). This environment is characterized by deposition of biogenic pelagic silica tests (typical of facies 2) and low concentrations of transported detrital material (Fig. 12). Although the percentage of diagenetic versus depositional micrite cannot be quantified, the low amount of detrital silt and argillaceous clay minerals in the facies dominating this assemblage (facies 2) indicates that this is the most distal environment.

Distal Outer Ramp (FA2).—This facies assemblage is dominated by facies 1 (detrital-quartz-silt-bearing fMs) interbedded with rare facies 2 and 3 (and facies 7 in the southernmost location) (Table 5; Fig. 18). The environment is also dominated by micrite, derived from a combination of pelagic nannofossils and shallow-water bottom-current-transported carbonate derived from the northeastern carbonate factory (Figs. 2, 16). However, it is characterized by relatively high dilution from detrital

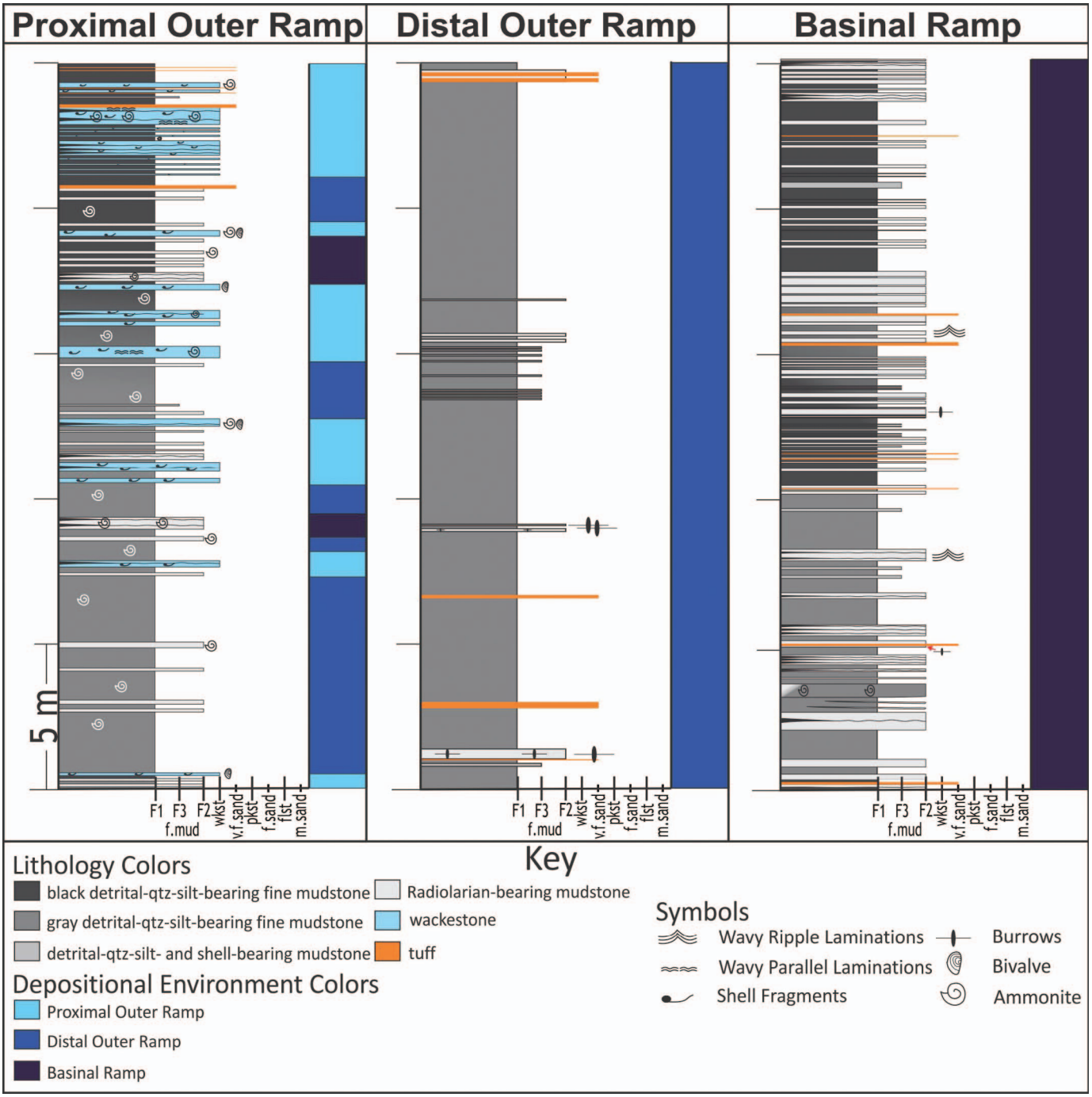

FIG. 18.—Lithologic logs characteristic of the three depositional sub-environments established in this study.

material derived from gravity flows moving northward and westward from the siliciclastic-dominated southern shoreline and deposition of relatively minor biogenic pelagic silica test input compared to the basinal ramp environment (Fig. 12). In the upper Pilmatué Member, facies 1 (four samples) shows an increase in illite and a decrease in carbonate. At the same stratigraphic positions, the southernmost locality contains isolated, discontinuous, bivalve-dominated floatstone beds (facies 6). A detailed taxonomic assessment was not conducted for this study, but generally these floatstone beds have a mixed bivalve assemblage that is dominated by oysters with possible inoceramids and *Pholadomya gigantea*. These floatstone beds are interpreted herein as local bioherms, suggesting a more proximal environment in the distal outer ramp. Analogous bivalve-dominated outer-ramp buildups have been documented in similar Cretaceous cratonic basins (Burchette and Wright 1992).

Proximal Outer Ramp (FA3).—This facies assemblage is dominated by facies 4, wackestone, interbedded with volumetrically minor amounts of facies 1 and 3, and even lesser amounts of facies 2 (Table 5; Fig. 18). The

TABLE 5.—*Facies assemblages of the Pilmatué and Agua de la Mula members within this study area.*

Facies Assemblage	Facies Present	Depositional Environment Interpretation
FA1	facies 2 dominant, minor facies 1 and facies 3 interbeds	Basinal Ramp
FA2	facies 1 dominant, minor facies 2 and facies 3 interbeds	Distal Outer Ramp
FA3	facies 4 dominant, minor facies 1 and facies 2 interbeds	Proximal Outer Ramp

environment is also dominated by micrite, derived from a combination of pelagic nannofossils and carbonate sourced from the northeastern carbonate factory and transported by shallow-water bottom currents, though to a lesser degree than in the distal outer ramp and basinal ramp (Figs. 2, 16). Additionally, the proximal outer ramp is characterized by the highest dilution of micritic matrix by sediment-gravity-flow-related detrital material and the coarsest-grained reworked macrofossil shell debris. This detrital material was likely sourced from the siliciclastic-dominated southern shoreline and suggests a more proximal, high-energy location compared to the distal outer ramp but still largely unaffected by storm activity (e.g., below storm wave base) (Fig. 12).

Global Implications

This study is one of only a handful that identifies a combination of pelagic suspension settling and dynamic current-influenced sedimentation below storm wave base in carbonate-dominated mudstone successions. The Eagle Ford Group (Cenomanian–Turonian, Western Interior Seaway) and the Vaca Muerta Formation (Late Jurassic, Neuquén Basin) are the two most notable examples that have recently been interpreted sedimentologically (Fairbanks et al. 2016; Frébourg et al. 2016; Minisini et al. 2018; Kietzmann et al. in press). The Eagle Ford Group is a classic example of a chalk–marl succession. However, the Agrio, with an accumulation rate approximately an order of magnitude greater than that of the Eagle Ford, is up to ~ 1,000 m thick, whereas the Eagle Ford is commonly ~ 60 m thick. Additionally, the source of carbonate mud is pelagic in the Eagle Ford, as opposed to pelagic and detrital (transported from the shallow carbonate factory) in the Agrio (Minisini et al. 2018). The Vaca Muerta and the Agrio are similar in that thick (~ 1000 m max) "deep"-water carbonate-dominated deposits (interbedded black shales, marls, and limestones) are found in the distal part of the basin (Kietzmann et al. 2014, 2016; Zeller et al 2015) and they are overall characterized by shallow-marine siliciclastic deposition that transitions to a shallow-marine carbonate ramp (Kietzmann et al. 2014).

The identification of currents in carbonate-dominated mudstone successions sub-storm wave base calls for a re-evaluation of simplistic facies models for interbedded chalk–marl or black shale–"pelagic" limestone successions worldwide. Despite a paradigm shift in the interpretation of mechanisms of mud deposition over the last decade from suspension settling alone to current-influenced sedimentation (Macquaker and Bohacs 2007; Schieber et al. 2007; Schieber et al. 2013), as it pertains to transported carbonate mud, most existing carbonate facies models still recognize only suspension settling of pelagically produced carbonate mud. In fact, as evidenced in the Agrio Formation here, pelagic carbonate mud may be reworked by currents sub-storm wave base. Additionally, neritically produced carbonate may be transported offshore to basinal environments. Literature on off-bank sediment-gravity-flow transport is well established (e.g., Goldstein et al. 2012), and there is a growing amount of current literature on carbonate slope processes and the reworking of sediment via contour currents (e.g., Eberli and Betzler 2019). Even so, existing literature on sediment gravity flows and contour currents are biased toward the documentation and interpretation of coarser-grained carbonate facies, with limited focus on carbonate mudstone facies. Future studies are needed to further test the origin and transport of carbonate mud deposited below storm wave base.

Source Potential

There have been a number of studies focused on the petroleum system of the Agrio Formation which utilize geochemical characterization of source potential to various degrees (Legarreta and Uliana 1991; Uliana and Legarreta 1993; Urien and Zambrano 1994; Cruz et al. 1996, 1998; Kozlowski et al. 1998; Uliana et al. 1999; Tyson et al. 2005; Spalletti et al. 2011). In general, the geochemical analyses of these studies rely on limited data points, focus almost exclusively on the basal section of the Agua de la Mula and Pilmatué members, and lack more than a very basic integration with stratigraphy and facies characterization. Previous work supports the overall increase in source potential from south to north in the Neuquén province that is suggested by the increase in S2 and HI values in the same direction across this study area (Tyson et al. 2005) (Fig. 13). The depositional model proposed for further testing herein sheds light on this trend, with the more siliciclastic shoreline-proximal southern localities receiving a higher proportion of original terrigenous organic matter (Fig. 2). Additionally, in the southern, more proximal part of the basin, organic matter may have been affected by a higher degree of degradation due to oxic conditions and/or increased bioturbation. Preferential degradation of the more labile marine organic compounds would lead to enrichment of the more molecularly stable terrigenous background organic matter (Hoefs et al. 2002; Sinninghe Damsté et al. 2002; Forster et al. 2008). An alternative explanation for the increase in source potential from south to north could be differential thermal degradation of kerogen based on maturity trends (Pepper and Corvi 1995a, 1995b; Pepper and Dodd 1995). A comparison of the thicknesses of the Pilmatué Member from the southern to the northern localities, ~ 500 m and ~ 260 m respectively, indicates that the southern localities would have experienced greater depositional burial depth, resulting in higher thermal maturity (Figs. 1C, 4). The higher thermal maturity in the southern localities could cause increased kerogen conversion behaviors, degrading the original or depositional source potential in this part of the basin. Though it is beyond the scope of this work, future studies could explore creating more detailed burial history models and establishing kinetic models specific to the Agrio Formation to correct the programmed pyrolysis data to original depositional values.

Previous outcrop- and well-based studies largely indicate that the basal sections of the Agua de la Mula Member, informally known as the "Spitidiscus shale," and the basal and upper sections of the Pilmatué Member in the more northern part of the basin have the highest source potential (Cruz et al. 1996, 1998; Kozlowski et al. 1998; Tyson 2001). By utilizing a much higher density of sample points collected from entire sections of each member in the part of the Neuquén province considered to have the highest source potential, this study is able to identify additional stratigraphic source intervals, SI2 and SI5, with well-constrained stratigraphic heights and thicknesses (Figs. 4, 14, 15). Furthermore, this study looks beyond TOC, applying filters for quality and type of organic matter, and linking geochemistry, facies (depositional), and stratigraphic patterns. An understanding of the vertical distribution of the proximal-to-distal trends established in the depositional model presented here in relation to these source intervals is the first step in establishing a robust

understanding of their position in the subsurface. Future work can focus on establishing a robust sequence stratigraphic framework based on a new understanding of mudstone facies variations and associated depositional environments.

CONCLUSIONS

In this study area, the greater part of the Pilmatué and Agua de la Mula members of the Agrio Formation consist dominantly of four volumetrically abundant facies, which are detrital-quartz-silt-bearing fine mudstone (facies 1), radiolarian-bearing calcareous fine mudstone (facies 2), detrital-quartz-silt- and shell-bearing calcareous fine mudstone (facies 3), and calcareous wackestone (facies 4).

Based on the facies interpretation and a paleogeographic understanding of the Neuquén Basin, three depositional mechanisms are recognized: 1) wave- and/or current-enhanced sediment gravity flows that delivered updip siliciclastic and bioclastic sediment to the offshore realm; 2) bottom-current-transported carbonate mud, sourced from the shallow marine carbonate factory and transported alongshore and oblique to shore by shallow-water, offshore-directed, bottom currents, and 3) production of pelagic and benthic tests, both calcareous and siliceous (i.e., nannofossils and microfossils). The facies are grouped into three facies assemblages, which are interpreted to have been deposited in a basinal ramp, distal outer ramp, or proximal outer ramp depositional environment. Utilizing previously established geochemical cutoffs, five source intervals have been identified in the Agua de la Mula and Pilmatué members at El Portón. The identification of stratigraphic source intervals and their potential to extend to the subsurface is innovative in a mudstone-dominated system such as the Agrio Formation.

Overall, facies variability, dominant current-influenced depositional mechanisms, and documented lateral shoreline variability all played a large role in the Agrio depositional system and have implications for source quality. This study provides a novel integration of sedimentology, stratigraphy, and inorganic and organic geochemical datasets, highlighting systematic facies heterogeneity that is critical to constructing an unconventional petroleum system model of the Agrio Formation and other similar carbonate-mudstone-dominated successions worldwide. Through detailed investigation, the results challenge the historical and simplistic depositional model for chalk–marl successions, recognizing a new level of complexity in carbonate mud transport and deposition below storm wave base.

SUPPLEMENTAL MATERIALS

Supplemental materials, Appendices A–D, are available from SEPM's data archive: https://www.sepm.org/supplemental-materials.

ACKNOWLEDGEMENTS

Sponsorship for this project was provided by Shell. The authors would like to thank Fernando Sanchez-Ferrer, Pedram Zarian, and Orlando Ortega from Shell for their discussions. David Thul was critical in establishing this research project, securing funding, creating collaborations between research groups, and planning field campaigns. We thank Adolfo Giusiano, the director (now retired) of the Hydrocarbon Secretariat of Neuquén Province, Argentina for sharing his expertise on the Neuquén Basin and the Agrio Formation, as well as helping the authors design and carry out a field campaign. Thanks to Magalí Alonso, Hydrocarbon Secretariat of Neuquén Province, for help with early field work. Alex Koch and Jessica Page were also key to the successful field work carried out for this project. We thank Chris Carlson, Clay Jones, and Joe Moore for allowing us to use the Energy and Geoscience Institute (EGI) XRD lab and for quantifying the XRD data. Dhrupad Beti performed critical quality control on programmed pyrolysis data and helped oversee use of the HAWK at EGI. David Watkins, University of Nebraska–Lincoln, provided key identifications and descriptions of nannofossil species. Additional student research grants were received to support the study from the SEPM (Society for Sedimentary Geology) Foundation Research Grant (S.A. Moore 2014), and the American Association of Petroleum Geologists (AAPG) Grants-in-Aid Harry and Joy Jamison Named Grant (S.A. Moore 2014).

REFERENCES

Abrams, M.A., and Thomas, D., in press, Geochemical evaluation of oil and gas samples from the Upper Devonian and Mississippian reservoirs southern Anadarko Basin Oklahoma and its implication for the Woodford Shale unconventional play: Marine and Petroleum Geology, doi:10.1016/j.marpetgeo.2019.104043.

Aguirre-Urreta, M.B., and Rawson, P.F., 1997, The ammonite sequence in the Agrio Formation (Lower Cretaceous), Neuquén Basin, Argentina: Geological Magazine, v. 134, p. 449–458.

Aguirre-Urreta, M.B., Concheyro, A., Lorenzo, M., Ottone, E.G., and Rawson, P.F., 1999, Advances in the biostratigraphy of the Agrio Formation (Lower Cretaceous) of the Neuquén Basin, Argentina: ammonites, palynomorphs, and calcareous nannofossils: Palaeogeography, Palaeoclimatology, Palaeoecology, v. 150, p. 33–47, doi:10.1016/S0031-0182(99)00006-1.

Aguirre-Urreta, M.B., Rawson, P.F., Concheyro, G.A., Bown, P.R., and Ottone, E.G., 2005, Lower Cretaceous (Barriasian–Aptian) biostratigraphy of the Neuquén Basin, *in* Veiga, G.D., Spalletti, L.A., Howell, J.A., and Schwarz, E., eds., The Neuquén Basin, Argentina: A Case Study in Sequence Stratigraphy and Basin Dynamics: Geological Society of London, Special Publication 252, p. 57–81.

Aguirre-Urreta, M.B., Lescano, M., Schmitz, M.D., Tunik, M., Concheyro, A., Rawson, P.F., and Ramos, V.A., 2015, Filling the gap: new precise Early Cretaceous radioisotopic ages from the Andes: Geological Magazine, v. 152, no. 3, p. 557–564, doi:10.1017/S0016756814000082X.

Aguirre-Urreta, M.B., Schmitz, M., Lescano, M., Tunik, M., Rawson, P.F., Concheyro, A., Buhler, M., and Ramos, V.A., 2017, A high precision U–Pb radioisotopic age for the Agrio Formation, Neuquén Basin, Argentina: implications for the chronology of the Hauterivian Stage: Cretaceous Research, v. 75, p. 193–204, doi:10.1016/j.cretres.2017.03.027.

Al Ibrahim, M.A., Sarg, J.F., Hurley, N., Cantrell, D.L., and Humphrey, J.D., 2017, Depositional environments and sequence stratigraphy of carbonate mudrocks using conventional geologic observations, multiscale electrofacies visualization, and geochemical analysis: the case of the Tuwaiq Mountain and Hanifa formations in a basinal setting, Saudi Arabia: American Association of Petroleum Geologists, Bulletin, v. 101, p. 683–714, doi:10.1306/08051615221.

Aplin, A.C., and Macquaker, J.H.S., 2011, Mudstone diversity: origin and implications for source, seal, and reservoir properties in petroleum systems: American Association of Petroleum Geologists, Bulletin, v. 95, p. 2031–2059, doi:10.1306/03281110162.

Back, S., Van Gent, H., Reuning, L., Grötsch, J., Niederau, J., and Kukla, P., 2011, 3D seismic geomorphology and sedimentology of the Chalk Group, southern Danish North Sea: Geological Society of London Journal, v. 168, p. 393–406, doi:10.1144/0016-76492010-047.3D.

Bathurst, R.G.C., 1975, Carbonate Sediments and Their Diagenesis, Second Edition: Amsterdam, Elsevier, 652 p.

Betzler, C., Lüdmann, T., Hübscher, C., and Fürstenau, J., 2013, Current and sea-level signals in periplatform ooze (Neogene, Maldives, Indian Ocean): Sedimentary Geology, v. 290, p. 126–137, doi:10.1016/j.sedgeo.2013.03.011.

Betzler, C., Lindhorst, S., Eberli, G.P., Lüdmann, T., Möbius, J., Ludwig, J., Schutter, I., Wunsch, M., Reijmer, J.J.G., and Hübscher, C., 2014, Periplatform drift: the combined result of contour current and off-bank transport along carbonate platforms: Geology, v. 42, p. 871–874, doi:10.1130/G35900.1.

Bhattacharya, J.P., and MacEachern, J.A., 2009, Hyperpycnal rivers and prodeltaic shelves in the Cretaceous Seaway of North America: Journal of Sedimentary Research, v. 79, p. 184–209.

Birdwell, J.E., Warden, A., Lewan, M.D., Lillis, P.G., and Dreier, M.F., 2017, Interlaboratory comparison of programmed pyrolysis data generated by different instruments: a case study on the Barnett Shale: Gulf Coast Association of Geological Societies, Transactions, v. 67, p. 405–406.

Birgenheier, L.P., Horton, B., McCauley, A.D., Johnson, C.L., and Kennedy, A., 2017, A depositional model for offshore deposits of the lower Blue Gate Member, Mancos Shale, Uinta Basin, Utah, USA: Sedimentology, v. 64, p. 1402–1438, doi:10.1111/sed.12359.

Bohacs, K.M., Grabowski, G.J., Jr., Carroll, A.R., Mankiewicz, P.J., Miskell-Gerhardt, K.J., Schwalbach, J.R., Wegner, M.B., and Simo, J.A., 2005, Production, destruction, and dilution: the many paths to source rock development, *in* Harris, N.B., ed., Deposition of Organic-Carbon-Rich Sediments: Models, Mechanisms, and Consequences, SEPM, Special Publication 82, p. 61–101, doi: 10.2110/pec.05.82.0061.

Bornemann, A., Aschwer, U., and Mutterlose, J., 2003, The impact of calcareous nannofossils on the pelagic carbonate accumulation across the Jurassic–Cretaceous boundary: Palaeogeography, Palaeoclimatology, Palaeoecology, v. 199, p. 187–228, doi:10.1016/S0031-0182(03)00507-8.

Breyer, J.A., 2016, The Eagle Ford Shale: A Renaissance in U.S. Oil Production: American Association of Petroleum Geologists, Memoir 110, 389 p.

Burchette, T.P., and Wright, V.P., 1992, Carbonate ramp depositional systems: Sedimentary Geology, v. 79, p. 3–57.

Burgess, P., Flint, S., and Johnson, S., 2000, Sequence stratigraphic interpretation of turbiditic strata: an example from Jurassic strata of the Neuquén Basin, Argentina: Geological Society of America, Bulletin, v. 112, p. 1650–1666.

Calvert, S.E., Bustin, R.M., and Ingall, E.D., 1996, Influence of water column anoxia and sediment supply on the burial and preservation of organic carbon in marine shales: Geochimica et Cosmochimica Acta, v. 60, p. 1577–1593.

Comerio, M., Fernández, D.E., and Pazos, P.J., 2018, Sedimentological and ichnological characterization of muddy storm related deposits: the upper Hauterivian ramp of the Agrio Formation in the Neuquén Basin, Argentina: Cretaceous Research, v. 85, p. 78–94, doi:10.1016/j.cretres.2017.11.024.

Cruz, C.E., Villar, H.J., and Muñoz, G.E., 1996, Los sistemas petroleros del Grupo Mendoza en La Fosa de Chos Malal: XII Congreso Geológico Argentino y III Congreso de Exploración de Hidrocarburos, Actas I, p. 45–60.

Cruz, C.E., Kozlowski, E., and Villar, H.J., 1998, Agrio (Neocomian) petroleum systems: main target in the Neuquén Bain Thrust Belt, Argentina, *in* Mello, M.R., and Yilmaz, P.O., eds., American Association of Petroleum Geologists, International Conference and Exhibition, Rio de Janeiro, Extended Abstracts, p. 670–671.

Demaison, G.J., and Moore, G.T., 1980, Anoxic environments and oil source bed genesis: American Association of Petroleum Geologists, Bulletin, v. 64, p. 1179–1209.

Denommee, K.C., Bentley, S.J., Harazim, D., and Macquaker, J.H.S., 2016, Hydrodynamic controls on muddy sedimentary-fabric development on the southwest Louisiana subaqueous delta: Marine Geology, v. 382, p. 162–175.

Dunham, R.J., 1962, Classification of carbonate rocks according to depositional texture, *in* Ham, W.E., ed., Classification of Carbonate Rocks: American Association of Petroleum Geologists, Memoir 1, p. 108–121.

Eberli, G.P., and Betzler, C., 2019, Characteristics of modern carbonate contourite drifts: Sedimentology, v. 66, p. 1163–1191, doi:10.1111/sed.12584.

Egenhoff, S.O., and Fishman, N.S., 2013, Traces in the dark: sedimentary processes and facies gradients in the upper shale member of the Upper Devonian–Lower Mississippian Bakken Formation, Williston Basin, North Dakota, U.S.A.: Journal of Sedimentary Research, v. 83, p. 803–824.

Eldrett, J.S., Ma, C., Bergman, S.C., Ozkan, A., Minisini, D., Lutz, B., Jackett, S.J., Macaulay, C., and Kelly, A.E., 2015, Origin of limestone–marlstone cycles: astronomic forcing of organic-rich sedimentary rocks from the Cenomanian to early Coniacian of the Cretaceous Western Interior Seaway, USA: Earth and Planetary Science Letters, v. 423, p. 98–113, doi:10.1016/j.epsl.2015.04.026.

Fairbanks, M.D., Ruppel, S.C., and Rowe, H., 2016, High-resolution stratigraphy and facies architecture of the Upper Cretaceous (Cenomanian–Turonian) Eagle Ford Group, Central Texas: American Association of Petroleum Geologists, Bulletin, v. 100, p. 379–403, doi:10.1306/12071514187.

Forster, A., Kuypers, M.M.M., Turgeon, S.C., Brumsack, H., Rose, M., and Sinninghe Damsté, J. S., 2008, The Cenomanian–Turonian oceanic anoxic event in the South Atlantic: new insights from a geochemical study of DSDP Site 530A: Palaeogeography, Palaeoclimatology, Palaeoecology, v. 267, p. 256–283, doi:10.1016/j.palaeo.2008.07.006.

Frank, T.D., Arthur, M.A., and Dean, W.E., 1999, Diagenesis of Lower Cretaceous pelagic carbonates, North Atlantic: paleoceanographic signals obscured: Journal of Foraminiferal Research, v. 29, p. 340–351.

Frébourg, G., Ruppel, S.C., Loucks, R.G., and Lambert, J., 2016, Depositional controls on sediment body architecture in the Eagle Ford–Boquillas system: insights from outcrops in west Texas, United States: American Association of Petroleum Geologists, Bulletin, v. 100, p. 657–682, doi:10.1306/12091515101.

Gabbott, S.E., Zalasiewicz, J.A., Aldridge, R.J., and Theron, J.N., 2010, Eolian input into the Late Ordovician postglacial Soom Shale, South Africa: Geology, v. 38, p. 1103–1106.

Gischler, E., and Zingeler, D., 2002, The origin of carbonate mud in isolated carbonate platforms of Belize, Central America: International Journal of Earth Sciences, v. 91, p. 1054–1070, doi:10.1007/s00531-002-0288-5.

Goldstein, R.H., Franseen, E.K., Dvoretsky, R.A., and Sweeney, R.J., 2012, Controls on focused-flow and dispersed-flow deepwater carbonates: Miocene Agua Amarga Basin, Spain: Journal of Sedimentary Research, v. 82, p. 499–520.

Gulisano, C.A., Gutiérrez Pleimling, A.R., and Digregorio, R.E., 1984, Esquema estratigráfico de la secuencia jurásica del oeste de la provincia del Neuquén: IX Congreso Geológico Argentino, San Carlos de Bariloche, Actas 1, p. 236–259.

Hammes, U., Hamlin, H.S., and Ewing, T.E., 2011, Geologic analysis of the Upper Jurassic Haynesville Shale in east Texas and west Louisiana: American Association of Petroleum Geologists, Bulletin, v. 95, p. 1643–1666, doi:10.1306/02141110128.

Hampson, G.J., 2000, Discontinuity surfaces, clinoforms, and facies architecture in a wave-dominated, shoreface–shelf parasequence: Journal of Sedimentary Research, v. 70, p. 325–340, doi:10.1306/2DC40914-0E47-11D7-8643000102C1865D.

Hoefs, M.J.L., Rijpstra, W.I.C., and Sinninghe Damsté, J.S., 2002, The influence of oxic degradation on the sedimentary biomarker record, I: evidence from Madeira Abyssal Plain turbidites: Geochimica et Cosmochimica Acta, v. 66, p. 2719–2735.

Hogancamp, N.J., and Pocknall, D.T., 2018, The biostratigraphy of the Bakken Formation: a review and new data: Stratigraphy, v. 15, p. 197–224, doi:10.29041/strat.15.3.197-224.

Howell, J.A., Schwarz, E., Spalletti, L.A., and Veiga, G.D., 2005, The Neuquén Basin: an overview, *in* Veiga, G.D., Spalletti, L.A., Howell, J.A., and Schwarz, E., eds., The Neuquén Basin, Argentina: A Case Study in Sequence Stratigraphy and Basin Dynamics: Geological Society of London, Special Publication 252, p. 1–14.

Immenhauser, A., 2009, Estimating palaeo–water depth from the physical rock record: Earth-Science Reviews, v. 96, p. 107–139, doi:10.1016/j.earscirev.2009.06.003.

Ingall, E.D., Bustin, R.M., and Van Cappellen, P., 1993, Influence of water column anoxia on the burial and preservation of carbon and phosphorus in marine shales: Geochimica et Cosmochimica Acta, v. 57, p. 303–316.

Johnston, D.I., Henderson, C.M. and Schmidt, M.J., 2010, Upper Devonian to Lower Mississippian conodont biostratigraphy of uppermost Wabamun Group and Palliser Formation to lowermost Banff and Lodgepole formations, southern Alberta and southeastern British Columbia, Canada: implications for correlations and sequence stratigraphy: Bulletin of Canadian Petroleum Geology, v. 58, p. 295–341, doi: 10.2113/gscpgbull.58.4.295.

Kietzmann, D.A., Palma, R.M., Riccardi, A.C., Martín-Chivelet, J., and López-Gómez, J., 2014, Sedimentology and sequence stratigraphy of a Tithonian–Valanginian carbonate ramp (Vaca Muerta Formation): a misunderstood exceptional source rock in the Southern Mendoza area of the Neuquén Basin, Argentina: Sedimentary Geology, v. 302, p. 64–86, doi:10.1016/j.sedgeo.2014.01.002.

Kietzmann, D.A., Ambrosio, A.L., Suriano, J., Alonso, M.S., Tomassini, F.G., Depine, G., and Repol, D., 2016, The Vaca Muerta–Quintuco system (Tithonian–Valanginian) in the Neuquén Basin, Argentina: a view from the outcrops in the Chos Malal fold and thrust belt: American Association of Petroleum Geologists, Bulletin, v. 100, p. 743–771, doi:10.1306/02101615121.

Kietzmann, D.A., Tomassini, F.G., and Smith, T., in press, Lithofacies and microfacies of the Vaca Muerta Formation based on subsurface and outcrop data, *in* Minisini, D., Fantin, M., Lanusse, I., and Leanza, H., eds., Integrated Geology of Unconventionals: The Case of the Vaca Muerta Play, Argentina: American Association of Petroleum Geologists, Memoir 120.

Kozlowski, E., Cruz, C.E., and Sylwan, C., 1998, Modelo exploratorio en la faja corrida de la Cuenca Neuquina, Argentina: Boletín de Informaciones Petroleras, v. 55, p. 4–23.

Lazar, O.R., Bohacs, K.M., Macquaker, J.H.S., Schieber, J., and Demko, T.M., 2015, Capturing key attributes of fine-grained sedimentary rocks in outcrops, cores, and thin sections: nomenclature and description guidelines: Journal of Sedimentary Research, v. 85, p. 230–246.

Lazo, D.G., 2004, Análisis de concentraciones fósiles del Cretácico Inferior de la Cuenca Neuquina [Ph.D. Thesis]: Universidad de Buenos Aires, 337 p.

Lazo, D.G., 2006, Análisis tafonómico e inferencia del grado de mezcla temporal y espacial de la macrofauna del Miembro Pilmatué de la Formación Agrio, Cretácico Inferior de cuenca Neuquina, Argentina: Ameghiniana, v. 43, p. 311–326.

Lazo, D.G., 2007a, Análisis de biofacies y cambios relativos del nivel del mar en el Miembro Pilmatué de la Formación Agrio, Cretácico Inferior de cuenca Neuquina, Argentina: Ameghiniana, v. 44, p. 73–89.

Lazo, D.G., 2007b, Early Cretaceous bivalves of the Neuquén Basin, west-central Argentina: notes on taxonomy, palaeobiogeography and palaeoecology: Geological Journal, v. 42, p. 127–142, doi:10.1002/gj.1080.

Lazo, D.G., Cichowolski, M., Rodríguez, D.L., and Aguirre-Urreta, M.B., 2005, Lithofacies, palaeoecology and palaeoenvironments of the Agrio Formation, Lower Cretaceous of the Neuquén Basin, Argentina, *in* Veiga, G.D., Spalletti, L.A., Howell, J.A., and Schwarz, E., eds., The Neuquén Basin, Argentina: A Case Study in Sequence Stratigraphy and Basin Dynamics: Geological Society of London, Special Publication 252, p. 295–315.

Lazo, D.G., Aguirre-Urreta, M.B., Price, G.D., Rawson, P.F., Ruffell, A.H., and Ogle, N., 2008, Palaeosalinity variations in the Early Cretaceous of the Neuquén Basin, Argentina: evidence from oxygen isotopes and palaeoecological analysis: Palaeogeography, Palaeoclimatology, Palaeoecology, v. 260, p. 477–493, doi:10.1016/j.palaeo.2007.12.008.

Leanza, H.A., Hugo, C.A., and Repol, D., 2001, Carta geológica de la Republica Argentina: SegemAR Instituto de Geología y Recursos Minerales, Zapala, no. 3969-I, scale 1:250.000.

Legarreta, L., Kozlowski, E., and Boll, A., 1981, Esquema estratigráfico y distribución de facies del Grupo Mendoza en el ámbito surmendocino de la Cuenca Neuquina: Actas VIII Congreso Geológico Argentino, v. 3, p. 389–409.

Legarreta, L., and Gulisano, C.A., 1989, Análisis estratigráfico secuencial de la cuenca Neuquina (Triásico Superior–Terciario Inferior), *in* Chebli, G.A., and Spalletti, L.A., eds., Cuencas Sedimentarias Argentinas: Serie de Correlación Geológica, v. 6, p. 221–243.

Legarreta, L., and Uliana, M.A., 1991, Jurassic–Cretaceous marine oscillations and geometry of backarc basin fill, central Argentine Andes, *in* MacDonald, D.I.M., ed., Sedimentation, Tectonics and Eustasy, Sea Level Changes at Active Margins: International Association of Sedimentologists, Special Publication, v. 12, p. 429–450.

Legarreta, L., and Uliana, M.A., 1999, El Jurásico y Cretácico de la Cordillera Principal y la Cuenca Neuquina, *in* Caminos, R., ed., Geología Argentina: Instituto de Geología y Recursos Minerales, Servicio Geológico Minero Argentino, Anales 29, p. 399–416.

Legarreta, L., and Villar, H.J., 2012, Las facies generadoras de hidrocarburos de la Cuenca Neuquina: Petrotecnia, v. Agosto, p. 14–39.

Legarreta, L., Villar, H.J., Laffitte, G.A., Cruz, C.E., and Vergani, G., 2005, Cuenca Neuquina: balance de masa enfocado a la evaluación del potencial exploratorio de los distritos productivos y de las zonas no productivas: VI Congreso de Exploración y Desarrollo de Hidrocarburos, p. 233–250.

Locklair, R., Sageman, B., and Lerman, A., 2011, Marine carbon burial flux and the carbon isotope record of Late Cretaceous (Coniacian–Santonian) Oceanic Anoxic Event III: Sedimentary Geology, v. 235, p. 38–49.

Lokier, S., and Steuber, T., 2008, Quantification of carbonate-ramp sedimentation and progradational rates for the late Holocene Abu Dhabi shoreline: Journal of Sedimentary Research, v. 78, p. 423–431.

MacEachern, J.A., Pemberton, S.G., Gingras, M.K., and Bann, K.L., 2010, Ichnology and facies models, *in* James, N.P., and Dalrymple, R.W., eds., Facies Models 4: St. John's, Newfoundland, Geological Society of Canada, p. 19–58.

Macquaker, J.H.S., and Bohacs, K.M., 2007, On the accumulation of mud: Science, v. 318, no. 5857, p. 1734–1735, doi:10.1126/science.1151980.

Macquaker, J.H.S., Bentley, S.J., and Bohacs, K.M., 2010a, Wave-enhanced sediment-gravity flows and mud dispersal across continental shelves: reappraising sediment transport processes operating in ancient mudstone successions: Geology, v. 38, p. 947–950.

Macquaker, J.H.S., Keller, M.A., and Davies, S.J., 2010b, Algal blooms and "marine snow": mechanisms that enhance preservation of organic carbon in ancient fine-grained sediments: Journal of Sedimentary Research, v. 80, p. 934–942, doi: http://doi.org/10.2110/jsr.2010.085.

Martinez, M., Pellenard, P., Deconinck, J.F., Monna, F., Riquier, L., Boulila, S., Moiroud, M., and Company, M., 2012, An orbital floating time scale of the Hauterivian–Barremian GSSP from a magnetic susceptibility signal (Río Argos, Spain): Cretaceous Research, v. 36, p. 106–115, doi:10.1016/j.cretres.2012.02.015.

Martinez, M., Deconinck, J.F., Pellenard, P., Riquier, L., Company, M., Reboulet, S., and Moiroud, M., 2015, Astrochronology of the Valanginian–Hauterivian stages (Early Cretaceous): chronological relationships between the Paraná–Etendeka large igneous province and the Weissert and the Faraoni events: Global and Planetary Change, v. 131, p. 158–173, doi:10.1016/j.gloplacha.2015.06.001.

McNeill, D.F., 2005, Accumulation rates from well-dated late Neogene carbonate platforms and margins: Sedimentary Geology, v. 175, p. 73–87, doi:10.1016/j.sedgeo.2004.12.032.

Minisini, D., Eldrett, J.S., Bergman, S.C., and Forkner, R., 2018, Chronostratigraphic framework and depositional environments in the organic-rich, mudstone-dominated Eagle Ford Group, Texas, USA: Sedimentology, v. 65, p. 1520–1557, doi:10.1111/ijlh.12426.

Morris, J.E., Hampson, G.J., and Johnson, H.D., 2006, A sequence stratigraphic model for an intensely bioturbated shallow-marine sandstone: the Bridport Sand Formation, Wessex Basin, UK: Sedimentology, v. 53, p. 1229–1263.

Neumann, A.C., and Land, L.S., 1975, Lime mud deposition and calcareous algae in the Bight of Abaco, Bahamas: a budget: Journal of Sedimentary Research, v. 45, p. 763–786, doi: 10.1306/212F6E3D-2B24-11D7-8648000102C1865D.

Nichols, G., 2009, Sedimentology and Stratigraphy, Second Edition: London, Blackwell Publishing, 419 p.

Pedersen, T.F., and Calvert, S.E., 1990, Anoxia vs. productivity: What controls the formation of organic-carbon-rich sediments and sedimentary rocks?: American Association of Petroleum Geologists, Bulletin, v. 74, p. 454–466.

Pemberton, S.G., MacEachern, J.A., Gingras, M.K., and Saunders, T.D.A., 2008, Biogenic chaos: cryptobioturbation and the work of sedimentologically friendly organisms: Palaeogeography, Palaeoclimatology, Palaeoecology, v. 270, p. 273–279, doi:10.1016/j.palaeo.2008.01.036.

Pepper, A.S., and Corvi, P.J., 1995a, Simple kinetic models of petroleum formation. Part I: oil and gas generation from kerogen: Marine and Petroleum Geology, v. 12, p. 291–319, doi:10.1016/0264-8172(95)98381-E.

Pepper, A.S., and Corvi, P.J., 1995b, Simple kinetic models of petroleum formation. Part III: modelling an open system: Marine and Petroleum Geology, v. 12, p. 417–452, doi:10.1016/0264-8172(95)96904-5.

Pepper, A.S., and Dodd, T.A., 1995, Simple kinetic models of petroleum formation. Part II: oil-gas cracking: Marine and Petroleum Geology, v. 12, p. 321–340, doi:10.1016/0264-8172(95)98382-F.

Peters, K.E., 1986, Guidelines for evaluating petroleum source rock using programmed pyrolysis: American Association of Petroleum Geologists Bulletin, v. 70, p. 318–329.

Peters, K.E., and Cassa, M.R., 1994, Applied source rock geochemistry, *in* Magoon, L.B., Dow, W.G., eds., The Petroleum System: From Source to Trap: American Association of Petroleum Geologists, Memoir 60, p. 93–120.

Peters, S.E., and Loss, D.P., 2012, Storm and fair-weather wave base: a relevant distinction?: Geology, v. 40, p. 511–514, doi:10.1130/G32791.1.

Phelps, R.M., Kerans, C., Da-Gama, R.O.B.P., Jeremiah, J., Hull, D., and Loucks, R.G., 2015, Response and recovery of the Comanche carbonate platform surrounding multiple Cretaceous oceanic anoxic events, northern Gulf of Mexico: Cretaceous Research, v. 54, p. 117–144, doi:10.1016/j.cretres.2014.09.002.

Plint, A.G., Tyagi, A., Hay, M.J., Varban, B.L., Zhang, H., and Roca, X., 2009, Clinoforms, paleobathymetry, and mud dispersal across the Western Canada Cretaceous Foreland Basin: evidence from the Cenomanian Dunvegan Formation and contiguous strata: Journal of Sedimentary Research, v. 79, p. 144–161, doi:10.2110/jsr.2009.020.

Rainoldi, A.L., Franchini, M., Beaufort, D., Patrier, P., Giusiano, A., Impiccini, A., and Pons, J., 2014, Large-scale bleaching of red beds related to upward migration of hydrocarbons: Los Chihuidos High, Neuquén Basin, Argentina: Journal of Sedimentary Research, v. 84, p. 373–393, doi: 10.2110/jsr.2014.31.

Ramos, V.A., and Folguera, A., 2005, Tectonic evolution of the Andes of Neuquén: Constraints derived from the magmatic arc and foreland deformation, *in* Veiga, G.D., Spalletti, L.A., Howell, J.A., and Schwarz, E., eds., The Neuquén Basin, Argentina: A Case Study in Sequence Stratigraphy and Basin Dynamics: Geological Society of London, Special Publication 252, p. 15–35.

Rossi, G.R., 2001, Arenisca Avilé: facies, ambientes sedimentarios y estratigrafía de una regresión forzada del Hauteriviano Inferior de la Cuenca Neuquina [Ph.D. Thesis]: Universidad Nacional de La Plata, Buenos Aires, Argentina, 331 p.

Sagasti, G., 2002, Estudio sedimentológico y de estratigrafía secuencial de las sedimentitas carbonáticas de la Formación Agrio (Cretácico inferior), en el sector surmendocino de la cuenca Neuquina, República Argentina [Ph.D. Thesis]: Universidad Nacional de La Plata, Buenos Aires, Argentina, 280 p.

Sagasti, G., 2005, Hemipelagic record of orbitally-induced dilution cycles in Lower Cretaceous sediments of the Neuquén Basin, *in* Veiga, G.D., Spalletti, L.A., Howell, J.A., and Schwarz, E., eds., The Neuquén Basin, Argentina: A Case Study in Sequence Stratigraphy and Basin Dynamics: Geological Society of London, Special Publication 252, p. 231–250.

Sagasti, G., and Ballent, S., 2002, Caracterización microfaunística de una transgresión marina: Formación Agrio (Cretácico inferior), Cuenca Neuquina, Argentina: Geobios, v. 35, p. 721–734.

Sageman, B.B., Murphy, A.E., Werne, J.P., Ver Straeten, C.A., Hollander, D.J., and Lyons, T.W., 2003, A tale of shales: the relative roles of production, decomposition, and dilution in the accumulation of organic-rich strata, Middle–Upper Devonian, Appalachian basin: Chemical Geology, v. 195, p. 229–273, doi:10.1016/S0009-2541(02)00397-2.

Sánchez, N.P., Coutand, I., Turienzo, M., Lebinson, F. Araujo, V., and Dimieri, L., 2018, Tectonic evolution of the Chos Malal Fold-and-Thrust Belt (Neuquén Basin, Argentina) from (U-Th)/He and fission track thermochronometry: Tectonics, v. 37, p. 1907–1929, doi: 10.1029/2018TC004981.

Schieber, J., 2016, Mud re-distribution in epicontinental basins: exploring likely processes: Marine and Petroleum Geology, v. 71, p. 119–133.

Schieber, J., Southard, J., and Thaisen, K., 2007, Accretion of mudstone beds from migrating floccule ripples: Science, v. 318, p. 1760–1763.

Schieber, J., Southard, J.B., Kissling, P., Rossman, B., and Ginsburg, R., 2013, Experimental deposition of carbonate mud from moving suspensions: importance of flocculation and implications for modern and ancient carbonate mud deposition: Journal of Sedimentary Research, v. 83, p. 1025–1031, doi:10.2110/jsr.2013.77.

Schieber, J., and Yawar, Z., 2009, New twist on mud deposition: mud ripples in experiment and rock record: The Sedimentary Record, v. 7, no. 2, p. 4–8, doi:10.1306/D4268AB8-2B26-11D7-8648000102C1865D.

Schmoker, J.W., 2002, Resource-assessment perspectives for unconventional gas systems: American Association of Petroleum Geologists, Bulletin, v. 86, p. 1993–1999.

Schwarz, E., Spalletti, L.A., and Veiga, G.D., 2011, La Formación Mulichinco (Valanginiano), *in* Leanza, H., Vallés, J., Arregui, C., and Danieli, J.C., eds., Relatorio del XVIII Congreso Geológico Argentino: Geología y Recursos Naturales de la Provincia del Neuquén, Actas I, v. 18, p. 131–144.

Schwarz, E., Spalletti, L.A., Veiga, G.D., and Fanning, C.M., 2016, First U-Pb SHRIMP age for the Pilmatué Member (Agrio Formation) of the Neuquén Basin, Argentina: implications for the Hauterivian lower boundary: Cretaceous Research, v. 58, p. 223–233, doi:10.1016/j.cretres.2015.10.003.

Schwarz, E., Veiga, G.D., Álvarez Trentini, G., Isla, M.F., and Spalletti, L.A., 2018, Expanding the spectrum of shallow-marine, mixed carbonate–siliciclastic systems: processes, facies distribution and depositional controls of a siliciclastic-dominated example: Sedimentology, v. 65, p. 1558–1589, doi:10.1111/sed.12438.

Sinninghe Damsté, J.S., Rijpstra, W.I.C., and Reichart, G.J., 2002, The influence of oxic degradation on the sedimentary biomarker record II: evidence from Arabian Sea sediments: Geochimica et Cosmochimica Acta, v. 66, p. 2737–2754.

Sonnenberg, S.A., 2011, The Niobrara petroleum system: a new resource play in the Rocky Mountain region, *in* Estes-Jackson, J.E., and Anderson, D.S., eds., Revisiting and Revitalizing the Niobrara in the Central Rockies: The Rocky Mountain Association of Geologists, p. 1–32.

Spalletti, L., Poiré, D.G., Pirrie, D., Matheos, S., and Doyle, P., 2001a, Respuesta sedimentológica a cambios en el nivel de base en una secuencia mixta clástica–carbonática del Cretácico de la Cuenca Neuquina, Argentina: Sociedad Geológica de España, Revista, v. 14, p. 57–74.

Spalletti, L.A., Poiré, D.G., Schwarz, E., and Veiga, G.D., 2001b, Sedimentologic and sequence stratigraphic model of a Neocomian marine carbonate–siliciclastic ramp: Neuquén Basin, Argentina: Journal of South American Earth Sciences, v. 14, p. 609–624, doi:10.1016/S0895-9811(01)00039-6.

Spalletti, L.A., Veiga, G.D., and Schwarz, E., 2011, La Formación Agrio (Cretácico Temprano) en la Cuenca Neuquina, *in* Leanza, H.A., Arregui, C., Carbone, O., Danieli, J.C., and Vallés, J.M., eds., Geología y Recursos Naturales de la Provincia del Neuquén: Relatorio del XVIII Congreso Geológico Argentino, p. 145–160.

Stow, D.A.V., Faugères, J.C., Howe, J.A., Pudsey, C.J., and Viana, A.R., 2002, Bottom currents, contourites and deep-sea sediment drifts: current state-of-the-art, *in* Stow, D.A.V., Pudsey, C.J., Howe, J.A., Faugères, J.C., and Viana, A.R., eds., Deep-Water Contourite Systems: Modern Drifts and Ancient Series, Seismic and Sedimentary Characteristics: Geological Society of London, Memoir 22, p. 7–20.

Taylor, A.M., and Goldring, R., 1993, Description and analysis of bioturbation and ichnofabric: Geological Society of London, Journal, v. 150, p. 141–148.

Taylor, J., and Sonnenberg, S.A., 2014, Reservoir characterization of the Niobrara Formation, southern Powder River Basin, Wyoming: The Mountain Geologist, v. 51, p. 83–108.

Tunik, M.A., Pazos, P.J., Impiccini, A., Lazo, D.G., and Aguirre-Urreta, M.B., 2009, Dolomitized tidal cycles in the Agua de la Mula Member of the Agrio Formation (Lower Cretaceous), Neuquén Basin, Argentina: Latin American Journal of Sedimentology and Basin Analysis, v. 16, p. 29–43.

Tunik, M., Folguera, A., Naipauer, M., Pimentel, M., and Ramos, V.A., 2010, Early uplift and orogenic deformation in the Neuquén Basin: constraints on the Andean uplift from U-Pb and Hf isotopic data of detrital zircons: Tectonophysics, v. 489, p. 258–273, doi:10.1016/j.tecto.2010.04.017.

Tyson, R.V., 2001, Sedimentation rate, dilution, preservation and total organic carbon: some results of a modelling study: Organic Geochemistry, v. 32, p. 333–339.

Tyson, R.V., and Pearson, T.H., 1991, Modern and ancient continental shelf anoxia: an overview, *in* Tyson, R.V., and Pearson, T.H., eds., Modern and Ancient Continental Shelf Anoxia: Geological Society of London, Special Publication 58, p. 1–24.

Tyson, R.V., Esherwood, P., and Pattison, K.A., 2005, Organic facies variations in the Valanginian–mid-Hauterivian interval of the Agrio Formation (Chos Malal area, Neuquén, Argentina): local significance and global context, *in* Veiga, G.D., Spalletti, L.A., Howell, J.A., and Schwarz, E., eds., The Neuquén Basin, Argentina: A Case Study in Sequence Stratigraphy and Basin Dynamics: Geological Society of London, Special Publication 252, p. 251–266.

Uliana, M.A., and Legarreta, L., 1993, Hydrocarbon habitat in a Triassic-to-Cretaceous sub-Andean setting: Neuquén Basin, Argentina: Journal of Petroleum Geology, v. 16, p. 397–420.

Uliana, M.A., Legarreta, L., Laffitte, G.A., and Villar, H.J., 1999, Estratigrafía y geoquímica de las facies generadoras de hidrocarburos en las cuencas petrolíferas de Argentina: IX Congreso de Exploración y Desarollo de Hidrocarburos, p. 3–92.

Urien, C.M., and Zambrano, J.J., 1994, Petroleum systems in the Neuquén Basin, Argentina, *in* Magoon, L.B., and Dow, W.G., eds., The Petroleum System: From Source to Trap: American Association of Petroleum Geologists, Memoir 60, p. 513–534.

Urien, C.M., Zambrano, J.J., and Yrigoyen, M.R., 1995, Petroleum basins of southern South America: an overview, *in* Tankard, A.J., Saruco, R.S., and Welsink, H.J., eds., Petroleum Basins of South America: American Association of Petroleum Geologists, Memoir 62, p. 63–77.

Van Dongen, B.E., Schouten, S., and Sinninghe Damsté, J.S., 2006, Preservation of carbohydrates through sulfurization in a Jurassic euxinic shelf sea: examination of the Blackstone Band TOC cycle in the Kimmeridge Clay Formation, UK: Organic Geochemistry, v. 37, p. 1052–1073.

Veiga, G.D., and Schwarz, E., 2017, Facies characterization and sequential evolution of an ancient offshore dunefield in a semi-enclosed sea: Neuquén Basin, Argentina: Geo-Marine Letters, v. 37, p. 411–426, doi:10.1007/s00367-016-0467-1.

Veiga, G.D., and Vergani, G.D., 1993, Depósitos de nivel bajo: nuevo enfoque sedimentológico y estratigráfico del Miembro Avilé en el Norte del Neuquén, Argentina, *in* Ramos, V.A., ed., XII Congreso Geológico Argentino y II Congreso de Exploración de Hidrocarburos, Actas I, p. 55–65.

Veiga, G.D., Spalletti, L.A., and Flint, S., 2002, Aeolian–fluvial interactions and high-resolution sequence stratigraphy of a non-marine lowstand wedge: the Avilé Member of the Agrio Formation (Lower Cretaceous), central Neuquén Basin, Argentina: Sedimentology, v. 49, p. 1001–1019.

Veiga, G.D., Howell, J.A., and Strömbäck, A., 2005, Anatomy of a mixed marine–non-marine lowstand wedge in a ramp setting. The record of a Barremian–Aptian complex relative sea-level fall in the central Neuquén Basin, Argentina, *in* Veiga, G.D., Spalletti, L.A., Howell, J.A., and Schwarz, E., eds., The Neuquén Basin, Argentina: A Case Study in Sequence Stratigraphy and Basin Dynamics: Geological Society of London, Special Publication 252, p. 139–162.

Veiga, G.D., Spalletti, L.A., and Flint, S.S., 2007, Anatomy of a fluvial lowstand wedge: the Avilé Member of the Agrio Formation (Hauterivian) in central Neuquén Basin (northwest Neuquén province), Argentina, *in* Nichols, G., Williams, E., and Paola, C., eds., Sedimentary Processes, Environments and Basins: A Tribute to Peter Friend: International Association of Sedimentologists, Special Publication 38, p. 341–365.

Veiga, G.D., Spalletti, L.A., and Schwarz, E., 2011, El Miembro Avilé de la Formación Agrio (Cretácico Temprano), *in* Leanza, H.A., Arregui, C., Carbone, O., Danieli, J.C., and Vallés, J.M., eds., Geología y Recursos Naturales de la Provincia del Neuquén: Relatorio del XVIII Congreso Geológico Argentino, p. 161–173.

Vergani, G.D., Tankard, A.J., Belotti, H.J., and Welsink, H.J., 1995, Tectonic evolution and paleogeography of the Neuquén Basin, Argentina, *in* Tankard. A.J., Saruco R.S., and Welsink, H.J, eds., Petroleum Basins of South America: American Association of Petroleum Geologists, Memoir 62, p. 383–402.

Villar, H.J., Laffitte, G.A., and Legarreta, L., 1998, The source rocks of the Mesozoic petroleum systems of Argentina: a comparative overview on their geochemistry, paleoenvironments and hydrocarbon generation patterns [Abstract]: International Congress and Exhibition of the American Association of Petroleum Geologists and the Brazilian Association of Petroleum Geologists, p. 186–187.

Weaver, C.E., 1931, Paleontology of the Jurassic and Cretaceous of West Central Argentina: Seattle, University of Washington Press, 469 p.

Werne, J.P., Sageman, B.B., Lyons, T.W., and Hollander, D.J., 2002, An integrated assessment of a "type euxinic" deposit: evidence for multiple controls on black shale deposition in the middle Devonian Oatka Creek Formation: American Journal of Science, v. 302, p. 110–143.

Westphal, H., Munnecke, A., Pross, J., and Herrle, J.O., 2004, Multiproxy approach to understanding the origin of Cretaceous pelagic limestone–marl alternations (DSDP site 391, Blake–Bahama Basin): Sedimentology, v. 51, p. 109–126.

Wilson, R.D., and Schieber, J., 2014, Muddy prodeltaic hyperpycnites in the lower Genesee Group of Central New York, USA: implications for mud transport in epicontinental seas: Journal of Sedimentary Research, v. 84, p. 866–874, doi:10.2110/jsr.2014.70.

Wilson, R.D., and Schieber, J., 2015, Sedimentary facies and depositional environment of the Middle Devonian Geneseo Formation of New York, U.S.A: Journal of Sedimentary Research, v. 85, p. 1393–1415, doi:10.2110/jsr.2015.88.

Zeller, M., Reid, S.B., Eberli, G.P., Weger, R.J., and Massaferro, J.L., 2015, Sequence architecture and heterogeneities of a field-scale Vaca Muerta analog (Neuquén Basin, Argentina): from outcrop to synthetic seismic: Marine and Petroleum Geology, v. 66, p. 829–847, doi:10.1016/j.marpetgeo.2015.07.021.

Zhao, J., Li, J., Wu, W., Cao, Q., Bai, Y., and Er, C., 2019, The petroleum system: a new classification scheme based on reservoir qualities: Petroleum Science, v. 16, p. 229–251, doi:10.1007/s12182-018-0286-2.

Zou, C.N., Yang, Z., Tao, S.Z., Yuan, X.J., Zhu, R.K., Hou, L.H., Wu, S.T., Sun, L., Zhang, G.S., Bai, B., Wang, L., Gao, X.H., and Pang, Z.L., 2013, Continuous hydrocarbon accumulation over a large area as a distinguishing characteristic of unconventional petroleum: the Ordos Basin, North-Central China: Earth-Science Reviews, v. 126, p. 358–369, doi:10.1016/j.earscirev.2013.08.006.

Received 31 May 2018; accepted 24 January 2020.